Sediment and carbon accumulation in a glacial lake in Chukotka (Arctic Siberia) during the late Pleistocene and Holocene: Combining hydroacoustic profiling and down-core analyses

Stuart A. Vyse[1,2], Ulrike Herzschuh[1,2,4], Gregor Pfalz[1,3], Lyudmila A. Pestryakova[5], Bernhard Diekmann[1,2,3],Norbert Nowaczyk[6], Boris K. Biskaborn[1]

[1]Alfred Wegener Institute Helmholtz Centre for Polar and Marine Research, Research Unit Potsdam, Telegrafenberg A45, 14471 Potsdam, Germany

[2]Institute of Environmental Science and Geography, University of Potsdam, Potsdam, Germany

[3]Institute of Geosciences, University of Potsdam, Potsdam, Germany

[4]Institute of Biochemistry and Biology, University of Potsdam, Potsdam, Germany

[5]Northeastern Federal University of Yakutsk, Yakutsk, Russia

[6]Helmholtz-Centre Potsdam GFZ, Climate Dynamics and Landscape Evolution, Telegrafenberg, 14473 Potsdam, Germany

*Correspondence to: **Stuart Andrew Vyse** (stuart.vyse@awi.de); **Boris K. Biskaborn** (boris.biskaborn@awi.de)*

Abstract

Lakes act as important sinks for inorganic and organic sediment components. However, investigations of sedimentary carbon budgets within glacial lakes are currently absent from Arctic Siberia. The aim of this paper is to provide the first reconstruction of accumulation rates, sediment and carbon budgets from a lacustrine sediment core from Lake Rauchuagytgyn, Chukotka (Arctic Siberia). We combined multiple sediment-biogeochemical and sedimentological parameters from a radiocarbon-dated 6.5 m sediment core with lake basin hydroacoustic data to derive sediment stratigraphy, sediment volumes, and infill budgets. Our results distinguished three principal sediment and carbon accumulation regimes that could be identified across all measured environmental proxies including Early MIS2 (ca. 29–23.4 cal. ka BP), Mid MIS2-early MIS1 (ca. 23.4–11.69 cal. ka BP), and Holocene (ca. 11.69– present). Estimated organic carbon accumulation rates (OCARs) were higher within Holocene sediments (average 3.53 g OC m^{-2} a^{-1}) than Pleistocene sediments (average 1.08 g OC m^{-2} a^{-1}) and are similar to those calculated for boreal lakes from Quebec and Finland and Lake Baikal but significantly lower than Siberian thermokarst lakes and Alberta glacial lakes. Using a bootstrapping approach, we estimated the total organic carbon pool to 0.26 ± 0.02 Mt and a total sediment pool of 25.7 ± 1.71 Mt within a hydroacoustically derived sediment volume of ca. 32990557 m^3. The total organic carbon pool is substantially smaller than Alaskan yedoma, thermokarst lake sediments, and Alberta glacial lakes but shares similarities with Finnish boreal lakes. Temporal variability in sediment and carbon accumulation dynamics at Lake Rauchuagytgyn is controlled predominantly by palaeoclimate variation that regulates lake ice-cover dynamics and catchment glacial, fluvial and permafrost processes through time. These processes, in turn, affect catchment and within-lake primary productivity as well as catchment soil development. Spatial differences to other lake systems at a trans-regional scale likely relates to the high-latitude, mountainous location of Lake Rauchuagytgyn.

1. Introduction

Lakes represent key sentinels of environmental change and can respond rapidly to changes in environmental conditions (Adrian et al., 2009). Lakes act as sinks of clastic sediment derived from local catchment weathering processes as well as from atmospheric deposition and as such gradually accumulate sediment mass over time (Dietze et al., 2014; Hinderer and Einsele, 2001). They also constitute a significant net sink of carbon, as they can accumulate organic and inorganic carbon within their sediments derived from allochthonous (lake external) and autochthonous (lake internal) pathways (Ferland et al., 2012; Dean and Gorham 1998; Kortelainen et al., 2004; Sobek et al., 2014). Recent syntheses suggest that global lakes represent a carbon sink of around 0.2–0.6 Pg C y^{-1} (Cole et al., 2007; Battin et al., 2009). In turn, inland waters can also act as major sources of the greenhouse gases CO_2 and CH_4 and thereby contribute further to global climate change (Anthony et al., 2014).

Lake sediment cores contain sedimentological and biogeochemical proxies of environmentally driven sedimentation and carbon dynamics (Birks and Birks, 2006; Biskaborn et al., 2019; Smol et al., 2002). When sedimentation rate data is available via dating of sediment cores, estimations of rates of sediment mass and carbon accumulation can be reconstructed (Ferland et al., 2012). Moreover, if the sediment volume stored within a lake basin can be estimated, sediment and carbon pools can be obtained that allows the lake function as a sediment and carbon sink to be assessed (Campbell et al., 2000; Lehman., 1975; Munroe & Brencher., 2019; Pajunen., 2000).

The region of Chukotka (Arctic Siberia) represents an environmentally sensitive area with limited lacustrine environmental reconstructions (Lozhkin and Anderson, 2013). Though a number of regional records across Arctic Siberia are becoming increasingly prevalent (Biskaborn et al., 2012; Diekmann et al., 2016; Melles et al., 2012; Pfalz et al., 2021; Subetto et al., 2017), studies have often neglected reconstructions of accumulation rates. This is largely due to limited age-controls related to problematic radiocarbon dating of organic poor systems that often lack dateable macrofossil remains and possess low dating resolutions (Lozhkin et al. 2016, Strunk et al., 2020). Current eastern Siberian research has primarily focussed on the reconstruction of Holocene accumulation rates of carbon using sediment cores derived from thermokarst lake systems (Anthony et al., 2014). Such studies have shown that lake systems may operate in transitional modes between carbon sink and source stages depending on the prevailing climatic background conditions (Anthony, et al., 2014). Recent syntheses have characterised the sedimentological characteristics and carbon budgets of Bykovsky peninsula lagoons of northern Yakutia, eastern Siberia and carbon inventories within alas and yedoma deposits from Central Yakutia and are interpreted in terms of palaeoenvironmental variability since the Pleistocene (Jenrich et al., accepted; Windirsch et al., 2020). Such works have also been extended to drained thermokarst lake basins (DTLB) and Pleistocene yedoma deposits in north-western Alaska (Jongejans et al., 2018). The reconstruction of accumulation rates in these syntheses has however been avoided due to significant reworking of carbon material within permafrost landscapes (Strunk et al., 2020; Windirsch et al., 2020). The role of Arctic Siberian glacial lakes as sediment and carbon sinks has not yet been accounted for.

Several, broad regional studies of dated sediment cores have been applied in an attempt to calculate accumulation rates and carbon pools within small glacial lakes in the Uinta mountains, north America (Munroe and Brencher, 2019) as well as in proglacial and bedrock-catchment lakes in southern Greenland (Anderson et al., 2009) and from large glacial lakes in Alberta, Canada (Campbell et al., 2000). A major drawback to these studies however is the absence or oversimplification of sediment volume estimation which does not account for

lateral variations in underlying sediment stratigraphy resulting from sediment focussing and winnowing (Ferland et al., 2012). Campbell et al. (2000) suggested an empirical equation for the estimation of sediment volume by simplifying lake sediments to an oblate semi-spheroid to account for sediment thinning at the lake margins. However, such approaches have been shown to lead to significant overestimations of sediment volumes and carbon pools up to four times the true value (Ferland et al., 2012; Munroe and Brencher, 2019). Hence the lack of efficient derivation of sediment volumes represents a major disadvantage of current works. Recent studies that include seismic or hydroacoustic based appraisals of sediment volume account for these disadvantages and show a major improvement of pool calculations (Einola et al., 2011; Ferland et al., 2012; Pajunen et al., 2000). Such methods are simple, rapid and give significant additional insight into lake bathymetry and basin-wide sediment stratigraphy that permits the retrieval of sediment thicknesses and volumes (Ferland et al., 2012). Recent hydroacoustic based studies from central and western Siberia have concentrated on determining Holocene and late Pleistocene sediment distributions and volumes within glacial lakes and have proven highly useful for understanding glacial history in these regions (Haflidason et al., 2019; Lebas et al., 2019). The inclusion of sediment budgets within investigations of carbon pools is important as it allows the future storage capacity of lakes to be estimated (Hinderer and Einsele, 2001).

This paper aims to provide a first estimation of late Pleistocene-Holocene sediment and carbon accumulation within an Arctic glacial lake basin within the remote Chukotka region (Arctic Siberia). This includes the first reconstruction of Pleistocene-Holocene sediment and organic carbon accumulation rates and pools provided for Chukotka derived by integrating proxy analyses from a high-resolution dated sediment core with high-resolution hydroacoustic data for sediment volumes. Our results are interpreted in the context of regional palaeoenvironmental variability during the late Pleistocene and are compared to trans-regional studies from Yakutia (east Siberia), North America and Europe. As such, our research questions are:

1. How has the palaeoenvironmental variability in Chukotka and resulting sedimentological processes since Marine Isotope Stage 2 (MIS2) influenced the sediment and carbon accumulation dynamics within an Arctic glacial lake?
2. How much sediment and carbon is stored within the Lake Rauchuagytgyn basin and how is this proportioned between the glacial and interglacial periods?
3. How do accumulation rates compare with other systems at a trans-regional scale?

2. Study area

Lake Rauchuagytgyn (67.7922° N, 168.7312° E) is situated within the glacially eroded U-shaped, Rauchua
mountain valley within the north-western Anadyr Mountains of Chukotka (Arctic Siberia) where elevations reach
up to 1600 m a.s.l (Fig. 1). The lake lies at an elevation of ca. 625 m a.s.l with a surface area of ca. 6.1 km^2 and
maximum water depth of 36 m. The lake is supplied by fluvial inflows at the lakes southern margin (Rauchua
River) and via an alluvial fan at the lakes south-eastern margin. One major outflow drains the lake to the north
and several minor streams drain the basin sides. The basin is divided into several sub-regions (southern and
south-eastern Inflows, southern sub-basin, northern sub-basin and northern shelf) based on water depth
characteristics. The catchment area comprises ca. 214.5 km^2. The bedrock surrounding the lake and within the
catchment is predominantly composed of cretaceous extrusive and intrusive igneous rocks consisting of silicic-
intermediate lithologies dominated by Andesite (Zhuravlev and Kazymin, 1999). Catchment evidence for
glaciation includes moraines to the north of the lake that denote the maximum extent of glaciation (Glushkova,
2011). Several small glacial cirques are found within the catchment (Glushkova, 2011) (Fig. 1a). The Arctic
continental climate of the area is characterised by mean annual temperatures of -11.8 °C and average July and
January temperatures of 13 °C and -30 °C, respectively with low annual precipitation of ca. 200 mm (Menne et
al., 2012). A surface ice-layer is present on lakes in this area from October to early July and likely reaches a
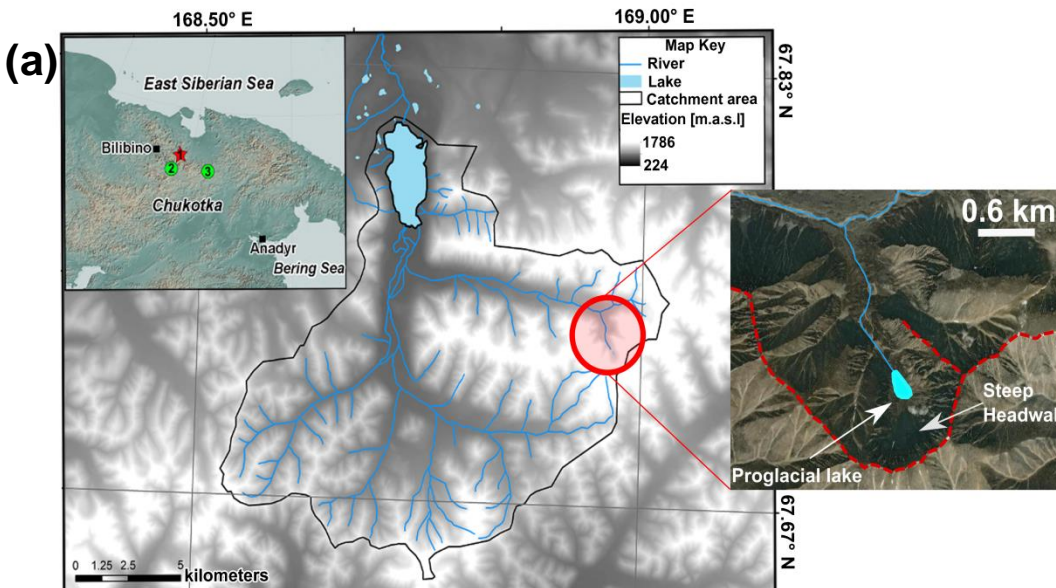
Figure 1. (a) Overview map of the Lake Rauchuagytgyn catchment plotted with a digital elevation map of the Anadyr mountains. In inset is shown the situation of Lake Rauchuagytgyn (1) compared to other studied regional lakes: (2) Lake Ilirney and (3) Lake El´gygytgyn (ESRI 2020). A second inset shows the outline of a glacial cirque associated with a small proglacial lake within the eastern catchment. (b) Orthophoto map of the lake and surrounding features. Shown are the locations of surface sampling points and the location of sediment core EN18218 (black dot) as well as an alluvial fan at the lakes south-eastern margin (ESRI 2020). Flow directions of major inflow and outflow river systems are shown (blue arrows). (c) Lake polygon with all hydroacoustic profile paths retrieved during 2018.

4
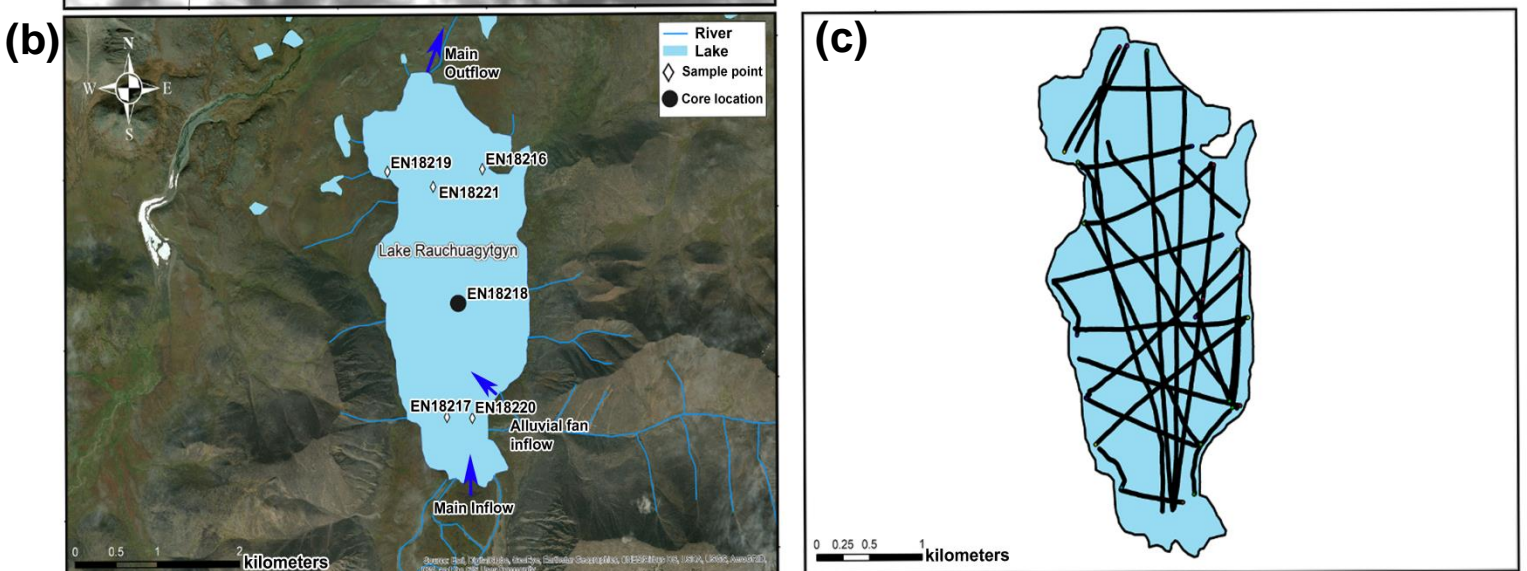
winter maximum thickness of ca. 1.8 m (Nolan et al., 2002). Catchment vegetation is dominated by open herb-
and graminoid tundra with no vegetation at higher elevations. Some forest tundra is found at lower elevations and
adjacent to river valleys (Shevtsova et al., 2020).

3. Materials and methods:

3.1 Fieldwork

Fieldwork took place at Lake Rauchuagytgyn in July 2018. An SES-2000 compact parametric sub-bottom profiler
was used to hydroacoustically survey the basin to identify major acoustic units (AUs) and sediment boundaries
and to locate an optimal coring location (Innomar technologies GmbH). A low frequency (8–10 kHz) and low
pulse interval (2 seconds) was used for high sediment penetration to retrieve sediment architecture. A high
frequency (100 kHz) and high pulse interval (253 microseconds) allowed derivation of lake bathymetry. Depth
conversion was conducted assuming a constant sound velocity of 1500 m s^{-1}. In total, 25 hydroacoustic profiles
containing > 23000 data points were retrieved.

Sediment core EN18218 (ca. 653 cm) (Fig. 1) was collected from the southern sub-basin using an UWITEC
piston coring system. The core was retrieved in parallel overlapping ca. 3 m segments, cut into 1 m sections and
transported in transparent 60 mm PVC tubes for further processing. Further core penetration and retrieval was
prevented by coarse material comprising of pebble-sized clasts at the core base that most likely represents the
lowermost deposited sediments within the basin.

Epilimnetic water samples were collected in 2016 (Huang et al., 2020) and in 2018 (this study) from multiple
surface locations and were immediately measured for pH, conductivity and oxygen content (WTW Multilab 540,
Germany). Water sub-samples were then filtered (0.45 μm) and transported for analyses of dissolved organic
carbon (DOC), anions and cations (Table S1).

3.2 Laboratory analyses

3.2.1 Core processing

Sediment cores were split into halves at the Alfred Wegener Institute Helmholtz Centre for Polar and Marine
Research (AWI) with one half being immediately subsampled for radiocarbon dating and subsequently at ca. 10
cm resolution for proxy analyses. The other half was cleaned and logged for macroscopic lithological changes
that permitted the derivation of three lithological units (LU-I to LU-III) and prepared for non-destructive scanning
approaches.

3.2.2 Radiocarbon dating and age-depth modelling

Due to the lack of suitable plant remains and low organic content of the retrieved sediment core, 25 bulk
sediment samples (0.5 cm thickness) and one surface sample (0–0.5 cm sediment depth) were dated for
radiocarbon using accelerator mass spectrometry (AMS) with the Mini Carbon Dating System (MICADAS) at AWI
Bremerhaven, Germany (Table 1). Samples were prepared following the standard MICADAS chemical
pretreatment procedure (see Gentz et al., 2017 for details).

The age-depth relationship was established by using the open-source MATLAB software package 'Undatable' (Lougheed and Obrochta, 2019). For modelling we used 23 bulk sediment samples. Two samples (Lab-ID: AWI - 3001.1.1; AWI - 3002.1.1) were slightly older than their successive dates further down, which suggest reworking in these depths (81.25 cm and 114.75 cm, respectively) and would lead to unrealistically high sedimentation rates when included within age-depth modelling that is not mirrored by sedimentological proxies. We treated these two dates as outliers and excluded them from the modelling process. All dates were calibrated to 'calibrated years Before Present' (years before 1950 C.E., 'cal. a BP') using the IntCal20 calibration curve (Reimer et al., 2020). In order to account for an existing age offset, we added the results from the surface sample (785 ± 31 ^{14}C years BP) to the software as reservoir age. Within 'Undatable', we set the parameters to the following values: nsim = 10^6, bootpc =70, xfactor = 0.1. Each parameter controls the behaviour of the age-depth model generation. The parameter "nsim" is responsible for the number of used iterations, "bootpc" controls the bootstrapping process, i.e., the outlier detection/uncertainty, and "xfactor" determines the uncertainty within the sedimentation accumulation rate between pairs of dating points (Lougheed and Obrochta, 2019). Median sedimentation rates (SR) (mm a^{-1}) were extracted from the final age-depth model. In order to account for age-depth model uncertainty in subsequent calculations, age-depth model derived 1σ and 2σ SR uncertainty ranges were also extracted.

Table 1. Radiocarbon dates from sediment core EN18218. Calibrated median ages and 2σ confidence intervals were calculated with CALIB 8.2 (Stuiver et al., 2020) using the IntCal20 (Reimer et al., 2020) calibration curve. Calibrated ages are given as calibrated years Before Present (years before 1950 C.E., 'cal yr BP'). The surface sample used for down-core correction of the reservoir effect was not calibrated. Samples in italic and marked with an asterisk (*) were excluded from the age-depth modelling.

Lab code	Sample ID	Composite depth (cm)	Radiocarbon age with error (^{14}C years BP)	Calibrated median age (cal. ^{14}C years BP)	Calibrated 2σ age range (cal. ^{14}C years BP)	Sample type
AWI - 5627.1.1	EN18218-1 Surface 0-0.5 cm	0.25	785 ± 31	-	-	Bulk, TOC
AWI - 2998.1.1	EN18218-2_0-100_20-20.5	18.75	2787 ± 33	2887	2783 – 2961	Bulk, TOC
AWI - 2999.1.1	EN18218-2_0-100_36.5-37	35.25	3629 ± 33	3942	3842 – 4080	Bulk, TOC
AWI - 3000.1.1	EN18218-2_0-100_61-61.5	59.75	3832 ± 33	4233	4098 – 4404	Bulk, TOC
*AWI - 3001.1.1**	*EN18218-2_0-100_82.5-83*	*81.25*	*4985 ± 33*	*5702*	*5602 – 5882*	*Bulk, TOC*
*AWI - 3002.1.1**	*EN18218-2_100-200_116-116.5*	*114.75*	*5417 ± 34*	*6234*	*6119 – 6295*	*Bulk, TOC*
AWI - 3003.1.1	EN18218-2_100-200_140-140.5	138.75	5074 ± 34	5816	5739 – 5908	Bulk, TOC
AWI - 3004.1.1	EN18218-2_100-200_164-164.5	162.75	5382 ± 34	6201	6008 – 6284	Bulk, TOC
AWI - 3005.1.1	EN18218-2_100-200_189-189.5	187.75	5852 ± 34	6672	6559 – 6746	Bulk, TOC
AWI - 3006.1.1	EN18218-2_200-240_222.5-223	221.75	6472 ± 35	7370	7310 – 7460	Bulk, TOC
AWI - 3007.1.2	EN18218-3_0-100_15-15.5	248.75	8872 ± 37	10011	9779 – 10177	Bulk, TOC
AWI - 3008.1.1	EN18218-3_0-100_37-37.5	270.75	9085 ± 37	10236	10185 – 10362	Bulk, TOC
AWI - 3009.1.1	EN18218-3_0-100_59.5-60	293.25	9516 ± 38	10827	10604 – 11074	Bulk, TOC
AWI - 3010.1.1	EN18218-3_0-100_83-83.5	316.75	9901 ± 39	11298	11214 – 11595	Bulk, TOC
AWI - 3011.1.1	EN18218-3_100-200_105-105.5	338.75	10197 ± 39	11866	11655 – 11994	Bulk, TOC
AWI - 3012.11	EN18218-3_100-200_129-129.5	362.75	11687 ± 30	13550	13481 – 13598	Bulk, TOC
AWI - 3013.1.1	EN18218-3_100-200_150-150.5	383.75	12205 ± 46	14112	14026 – 14310	Bulk, TOC
AWI - 3014.1.1	EN18218-3_100-200_171-171.5	404.75	13017 ± 48	15596	15371 – 15760	Bulk, TOC
AWI - 3015.1.1	EN18218-3_200-292_210-210.5	443.75	14330 ± 52	17427	17197 – 17803	Bulk, TOC
AWI - 3016.1.1	EN18218-3_200-292_239-239.5	474.75	15686 ± 48	18941	18847 – 19068	Bulk, TOC
AWI -	EN18218-3_200-	503.75	17708 ± 56	21473	21191 – 21783	Bulk,

7

3017.1.1	292_270-270.5					TOC
AWI - 3018.1.1	EN18218-4_0-100_35-35.5	536.25	18000 ±55	21945	21740 – 22117	Bulk, TOC
AWI - 3019.1.1	EN18218-4_0-100_64.5-65	565.75	22649 ±66	27059	26479 – 27226	Bulk, TOC
AWI - 3020.1.1	EN18218-4_0-100_95-95.5	596.25	21786 ±204	26077	25725 – 26442	Bulk, TOC
AWI - 3021.1.1	EN18218-4_100-163_123-123.5	624.25	25689 ±325	29941	29205 – 30735	Bulk, TOC
AWI - 3022.1.1	EN18218-4_100-163_145-145.5	646.25	25081 ±300	29393	28780 – 29978	Bulk, TOC

3.2.3 Sediment-geochemistry, Magnetic Susceptibility and Grain-Size

Semi-quantitative sediment geochemical data were obtained by X-ray fluorescence line-scanning (XRF) of EN18218 halves. XRF was carried out using an Avaatech core-scanner with a Rh X-ray tube at 0.75 mA and 1.5 mA for 10 and 15 seconds, at 10 kV (no-filter) and 30 kV (Pd-thick filter) at the Federal Institute for Geosciences and Natural Resources (BGR), Germany. A scanning resolution of 5 mm was chosen. The main rock-forming (Aluminium (Al), Silicon (Si), Calcium (Ca), Potassium (K), Titanium (Ti), Manganese (Mn), Iron (Fe), Rubidium (Rb), Strontium (Sr), Zircon (Zr)) and productivity (Bromine (Br)) linked elements were selected for further processing (Fig. S1). Of these single elements we focus primarily on Br, Ca, K and Ti within this study. The element ratio of K/Ti is used as proxy for clay input and chemical vs physical weathering (Arnaud et al., 2012; Cuven et al., 2010; Kilian et al., 2013; Marshall et al., 2011). Zr/K and Si/Al are included as proxies for coarser grain-sizes and Mn/Fe for redox conditions (Baumer et al., 2020; Cuven et al., 2010; Píšková et al., 2019). Br/Al is utilised alongside Br as a proxy for productivity (Lenz et al., 2020). Magnetic susceptibility measurements (MS) were carried out at 1 mm intervals using a Bartington MS2E spot reading sensor integrated in a fully automatic split-core logging device, developed at the GFZ Potsdam, Germany (Bartington Instruments Ltd). Core images and commission on Illumination (CIE) l* (lightness) and b* (blue-yellow) colour data were retrieved using an Avaatech line scan camera. XRF and MS data were smoothed using 5- and 15-point running means respectively.

Sediment grain-size analysis was performed on 63 core samples and four surface samples following a 3-week hydrogen peroxide (H_2O_2) treatment to remove organic matter. Samples were homogenised using an elution shaker for 24 hours and split into eight subsamples. At least three subsamples were analysed thrice providing overall nine individual measurements using a Malvern Mastersizer 3000 laser diffraction particle analyser (Malvern Panalytical Ltd). The nine measurements were then averaged to produce a grain-size distribution for each sample. Data was processed using „GRADISTAT" 8.0 software (Blott and Pye, 2001). Intervals of 2 mm–63 µm, 63–2 µm and <2 µm, were used to define percentages of sand, silt and clay respectively (Friedman and Sanders, 1978). The Folk and Ward method was used for mean grain-size calculation (Folk and Ward, 1957).

3.2.4 Dry bulk density, elemental analyses and accumulation rate calculations

Water contents (wt%) and dry bulk densities (DBD in g cm^{-3}) were determined using the volumetric approach of Avnimelech et al. (2001) on 63 samples of known volume obtained with a one cm^3 cube during subsampling and calculated from weight-loss following freeze-drying (See also Pajunen, 2000). The total sediment mass accumulation rate (MAR) in g cm^{-2} a^{-1} was calculated according to the ocean drilling project (ODP) methodology (http://www-odp.tamu.edu/) (Eq. 1).

$$MAR = DBD \times SR$$

(1)

Where DBD is dry bulk density and SR is age-depth model derived sedimentation rate (cm a^{-1}). MAR uncertainty ranges were determined by applying Eq. 1 to sedimentation rate 1σ and 2σ uncertainty ranges extracted from the age-depth model.

Subsequently, 65 dried and milled sub-samples were analysed for total organic carbon (TOC) and total inorganic carbon (TIC) using a Vario SoliTOC cube elemental analyser following combustion at 400 °C (TOC), and 900 °C

(TIC) (Elementar Corp., Germany). Total carbon (TC) was calculated as the total sum of TOC and TIC. Total sulphur (TS) was measured using an Eltra Carbon and Sulfur determinator (Eltra GmbH, Germany). Device results are given as weight percent (wt%) in relation to sample mass. Organic carbon accumulation rates (OCARs) were then calculated by combining TOC (wt%) & DBD to produce organic carbon content per volume (g OC cm^{-3}) and then with SR for each depth (Eq. 2).

$$OCAR = (DBD \times (\frac{TOC}{100})) \times SR$$

(2)

OCARs are reported as grams of organic carbon per square metre per year (g OC m^{-2} a^{-1}) for comparison with published organic carbon accumulation rates. OCAR uncertainty ranges were calculated identically to MAR uncertainty ranges.

Average SR, MAR and OCARs were determined for each lithological unit (LU) and the composite sediment succession.

3.3 Data analyses

3.3.1 Estimation of lake basin sediment volumes

Hydroacoustic profiles were processed and major hydroacoustic boundaries delineated using ISE2 2.9.5 software (Innomar technologies GmbH). Boundary depths were extracted using the ISE2 "Depth extraction" tool and were imported into ArcMap 10.5.1 software. Data gaps between measurement points and profiles were interpolated using the "Topo to Raster" tool to produce interpolated depth surfaces to the sediment-water interface and to basin-wide boundary surfaces (Supplement Fig. S3). The interpolated sediment-water interface depths were subtracted using the raster calculator tool from interpolated boundary depths to estimate total basin and acoustic unit sediment thicknesses (T$_{sediment}$). Sediment volumes (Vsediment) were subsequently derived from estimated sediment thicknesses using the "Surface Volume" tool (Table 2).

Table 2. Overview of general acoustic (AU) and lithological unit (LU) divisions w ith associated depth and age ranges and age-depth model calculated average sedimentation rates (SR). Additionally show n are basin properties calculated using ArcMap 10.5.1 softw are including Interpolated w ater and sediment thicknesses (T$_{water}$, T$_{sediment}$) and w ater and sediment package volumes (V$_{water}$, V$_{sediment}$).

Acoustic Unit (AU)	Lithological Unit (LU)	Depth range at core location (cm)	Age range (cal. ka BP)	Average Sedimentation rate (SR) (mm a^{-1})	Average Interpolated thickness (m) (T$_{water,}$ T$_{sediment}$)	Estimated volume (m^3) (V$_{water,}$ V$_{sediment}$)
Water	Water	-	-	-	14.5	90103775
1	I	0 - 346	0 - 11.69	0.36	2.44	14935205

10

2	II	LU-II = 346 - 560	11.69 – 23.4	0.20	2.96	18055352
	III	LU-III = 561 - 653	23.4 – ca. 29	0.17		

3.3.2 Estimation of carbon and sediment pools using bootstrapping

In order to estimate sediment (Sed_{pool}, Mt) and carbon pools (TOC_{pool}, Mt) at Lake Rauchuagytgyn, we used an
250 established bootstrapping approach modified from Strauss et al. (2013), Jongejans et al. (2018) and Windirsch et al. (2020) that excluded ice-wedges not present within the lake sediments and was enhanced to include sediment volumes estimated from GIS-based methods (Eq. 3 & 4).

$$Sed_{pool} = \frac{V_{sediment} \times DBD}{10^6}$$

(3)

$$TOC_{pool} = \frac{V_{sediment} \times DBD \times (\frac{TOC}{100})}{10^6}$$

(4)

255 The bootstrapping approach was carried out using the "boot" (version 1.3-25) and "Bootstrapping-permafrost-OC" packages (Jongejans and Strauss, 2020) in the R environment and included 10,000 iterations of random sampling and replacement of values (Davison and Hinkley, 1997). Combined DBD and TOC values were used for carbon pool estimation and simply DBD for the sediment pool. The approach was applied firstly to the entire sediment core and basin sediment volume and then individually for the LU-II/LU-III (AU2) and LU-I (AU1)
260 sediment packages. The mean sediment and carbon pools (in megatons, Mt), densities (Kg m^{-3}) and associated standard deviations and confidence intervals of all iterations were computed (See Strauss et al., 2013 for details) (Supplement S4 Code).

3.3.3 Multivariate statistics

In order to reduce data dimensionality and increase interpretability of presented physicochemical sediment
265 stratigraphic and accumulation rate data obtained from core EN18218, principal component analysis (PCA) was carried out following data centering and standardisation by dividing by standard deviation using the „prcomp" function in R (R Core team, 2013). Probability ellipses were drawn in the resulting PCA biplot for samples included within each lithological unit.

270

4. Results

4.1 Basin hydroacoustic stratigraphy and sediment distributions

Hydroacoustic and bathymetric data (Fig. 2) permit the division of the lake basin into four morphological regions: northern shelf, northern sub-basin, southern sub-basin and southern inflow (Fig. 3a). The basin is characterised by steep east and west margins and a central basin bathymetric high. A pronounced river delta is present at the southern lake margin at the major lake Inflow (Fig. 1b). An alluvial fan at the lakes south-eastern margin represents drainage from a steep, lake-proximal, west-east oriented valley (Fig. 1b). Hydroacoustic data allowed effective imaging of much of the sediment infill except within inflow proximal profiles where acoustic blanking limited data retrieval (Fig. 2b).
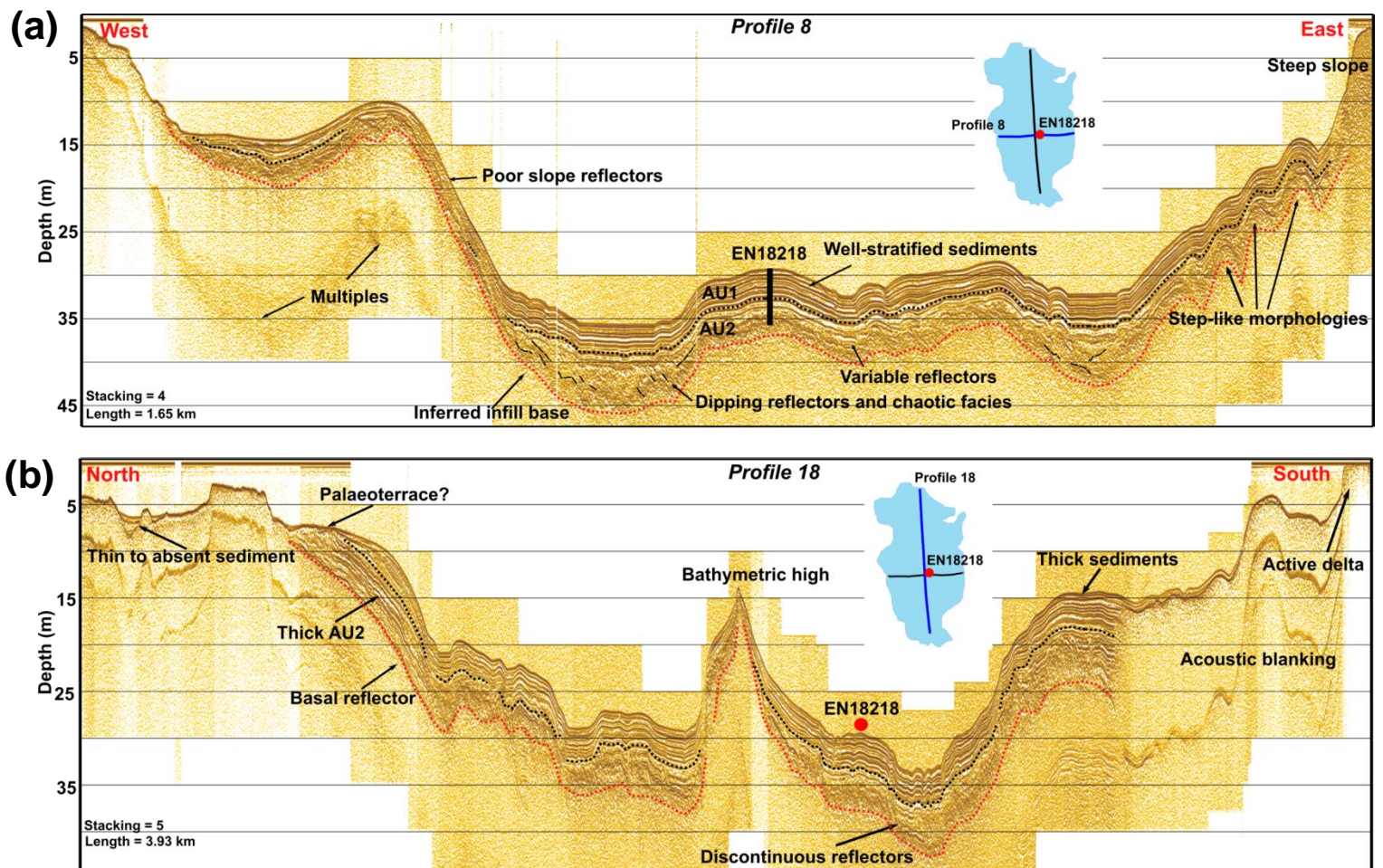

Figure 2. Interpreted hydro-acoustic profiles from Lake Rauchuagytgyn (Profile 8 and Profile 18). Both profiles pass close to the drilling location of EN18218. Shown are inferred major hydroacoustic boundaries defined that are connected with major lithological changes recorded by EN18218 and interpreted across the basin.

Average sediment thickness of the entire lake basin infill is estimated as ca. 5.33 m with the thickest infill predominantly within the southern sub-basin and generally correlates with greater water depth. Average total sediment thickness equates to a total sediment volume of ca. 32990557 m^3 (0.033 km^3) (Fig. 3d). Sediment thicknesses decrease towards the basin margins, particularly within the northern-shelf where water depths < 7.5 m show reduced sedimentation and evidence of ponded sediment lenses and erosion (Figs. 2b, 3b–d). Comparison of hydroacoustic with lithological data and boundaries from core EN18218 allow the subdivision of

12

basin infill into two acoustic units (AU1 & AU2) corresponding with sediments deposited within lithological units I (AU1) and II & III (AU2) (Table 2). The boundary between AU1 and AU2 represents a major lithological boundary. The base of AU2 likely constitutes the base of sediment infill and is marked by progressively weakening reflectors with depth. Both boundaries trace closely the modern-day lake bathymetry (Fig. S3). Acoustic reflectors within AU1 demonstrate generally well-stratified, high-amplitude, continuous, horizontal and sub-parallel reflectors bounded at the top by the sediment-water interface. The thickness of AU1 shows a basin-wide average of 2.44 m and is thickest within the southern sub-basin proximal to the fluvial inflow and alluvial fan (6.5–7 m) and thins towards the northern shelf (Fig. 3b). A volume of ca. 14935205 m^3 (0.015 km^3) was estimated for AU1.

Reflectors within the uppermost portion of AU2 show generally lower amplitude, sub-horizontal and sub-parallel reflectors and show some continuity with AU1 reflectors (Fig. 2a, b). The lowermost part of AU2 consists of highly discontinuous reflectors with little structure and rare sub-horizontal reflectors and likely includes coarse sediments consisting of pebble-sized clasts deposited at the bottom of LU-III directly at the core base and below. The upwards transition to sub-parallel reflectors likely represents sediments deposited within the majority of LU-III and throughout LU-II. AU2 is more variable in thickness (average ca. 2.96 m) than AU1 but is generally thickest within the southern sub-basin and to a lesser-extent within the northern sub-basin and at localities close to the northern shelf/northern sub-basin boundary observed within hydroacoustic profiles (Fig. 3c). AU2 possesses a volume of ca. 18055352 m^3 (0.018 km^3) with complex internal architecture with elevation and depression-like structures and ridges seen within some areas.
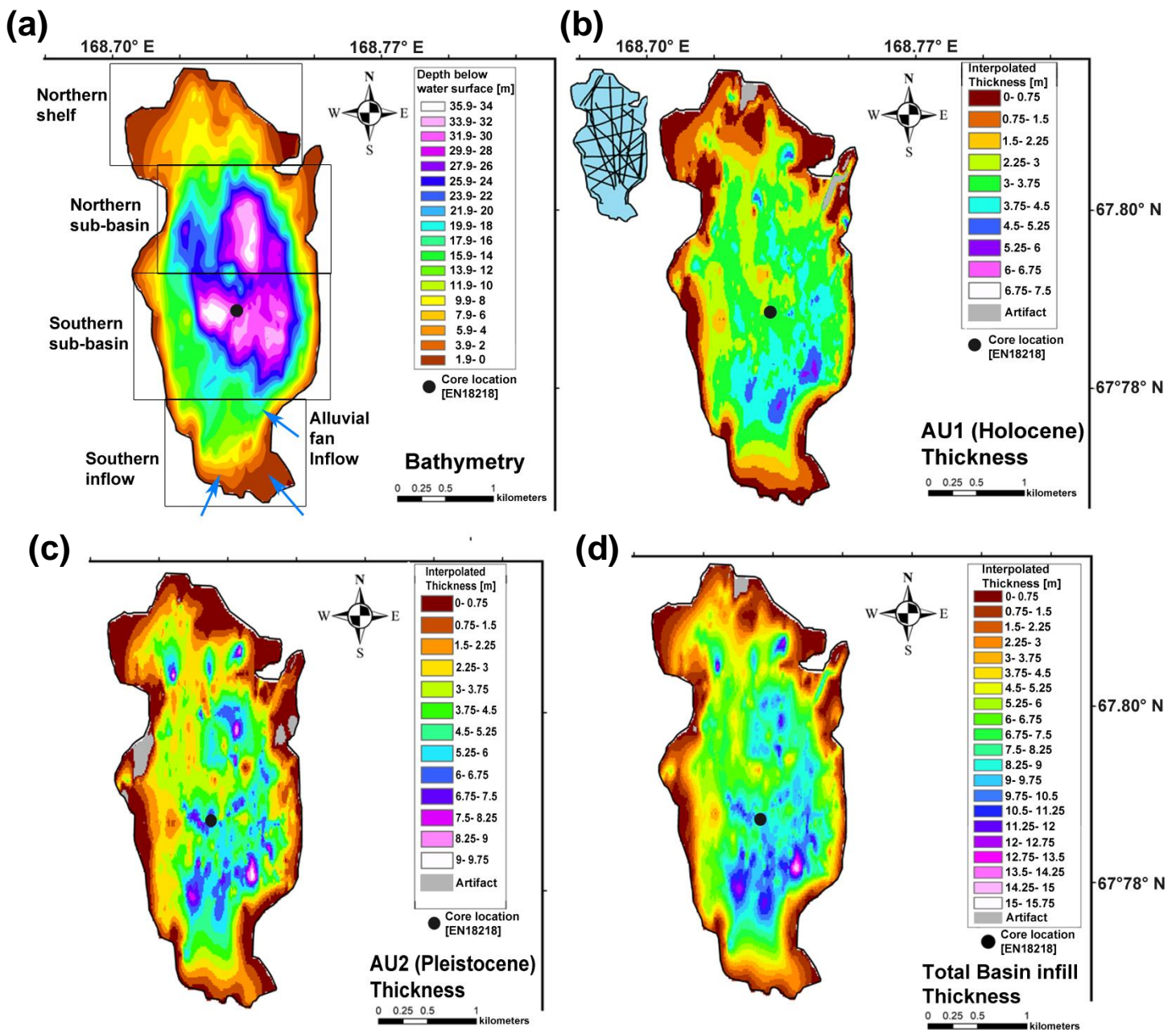
Figure 3. (a) Interpolated high-resolution lake bathymetry with morphological regions denoted by black boxes. **(b)** Interpolated AU1 thicknesses. Blue and pink colors denote the thickest sediment within the southern sub-basin. **(c)** Interpolated sediment thicknesses within AU2. Similarly to AU1, the greatest thicknesses are predominantly located in the southern sub-basin but with other locations in the northern-sub basin showing thick sediments too. **(d)** Whole sediment package interpolated thickness. Thin sediment is found proximal to the basin margins and at the north-western shelf. The sediment distribution generally reflects sediment focussing into the deeper lake at greater water depths. Interpolation artifacts are attributed to data sparsity and difficulty in tracing reflectors in some regions due to acoustic blanking that led to erroneous interpolation. Larger artifacts were hence excluded.

4.2 Core chronology and sedimentation rates

The age-depth model (Fig. 4a) shows maximum modelled sediment ages of ca. 29 cal. ka BP at the core base and thus the core provides an entire record of the Holocene and MIS2. Median sedimentation rates (SR) are plotted alongside 1σ and 2σ uncertainty ranges and vary from a maximum of 0.54 mm a^{-1} to a minimum of 0.12 mm a^{-1} (Fig. 4b). Sedimentation rates are highest within LU-I (average 0.36 mm a^{-1}, average 1σ uncertainty 0.25–0.45 mm a^{-1}). Low-intermediate but progressively increasing rates are seen within LU-II (average 0.20 mm a^{-1}, average 1σ uncertainty 0.16–0.23 mm a^{-1}) with pronounced peaks at 510.5 and 371 cm. LU-III demonstrates low rates, but with larger uncertainty (average 0.17 mm a^{-1}, average 1σ uncertainty 0.15–0.27 mm a^{-1}) due to age model scatter. Changes in sedimentation rates generally correspond with major lithological variations.

14

Sedimentation rate reductions occur at the LU-III/LU-II (ca. 560 cm) boundary and increases are observed across

320   the LU-II/LU-I (ca. 346 cm) boundary (Fig 4a, b).
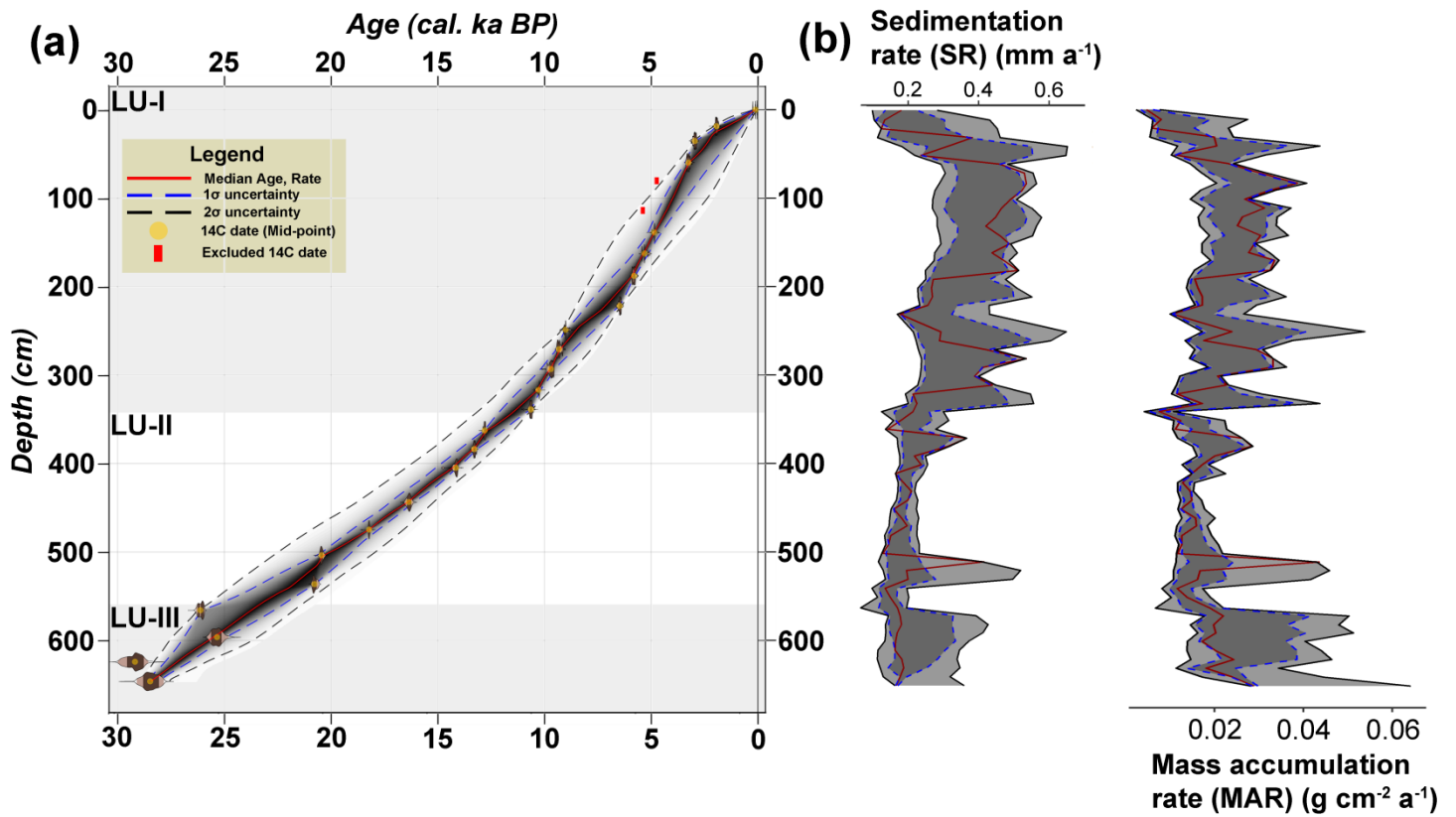
Figure 4. (a) High-resolution age-depth model for sediment core EN18218 created from 23 radiocarbon dates with sigma uncertainty range. **(b)** Sedimentation and mass accumulation rates (dark red lines) and 1 and 2σ uncertainty ranges (dark and light grey ribbons).

325

330

4.3 Core sedimentological and biogeochemical characteristics

LU-III (Table 2) represents the lowermost unit of core EN18218 and comprises very poorly sorted, coarse material consisting of pebble-sized clasts directly at the core base of LU-III (ca. 653 cm) that blocked further core retrieval. Coarse basal sediment is then succeeded by overlying, yellow-grey, light-coloured (low b*), and layered silty-clay sediments from ca. 653 cm to 560 cm. Sediments within LU-III show low water contents (average 39.5 %), high DBD (average 1.22 g cm^{-3}), very high magnetic susceptibility values (average 681 [10^{-6} SI]) and low mean grain-sizes (average 3.9 μm) traced by Zr/K, Si/Al and K/Ti ratios (Figs. 5, 6). The grain-size distribution shows a predominance of silt-clay with minor sand concentrated just above the core base (ca. 650.5 cm). MARs vary between 0.029 g cm^{-2} a^{-1} at the core base and 0.019 g cm^{-2} a^{-1} at the top of LU-III (average 0.022 g cm^{-2} a^{-1}, average 1σ uncertainty 0.019–0.034 g cm^{-2} a^{-1}) but are associated with high uncertainty in the positive sigma direction (Fig. 4). TOC contents (wt%) (average 0.27 %) and Br/Al ratio values demonstrate their lowest values within LU-III alongside TC (average 0.28 %) and TS (average 0.018 %) (Fig. 6). OCARs are extremely low and stable with low uncertainty (average 0.58 g OC m^{-2} a^{-1}, average 1σ uncertainty 0.50–0.92 g OC m^{-2} a^{-1}). Equally Mn/Fe shows stable, low values. The LU-III/LU-II boundary is characterised by a decrease in magnetic susceptibility and increase in the K/Ti ratio corresponding to finer grain-sizes at around 560 cm with a grain-size minimum (2.3 μm) at 550 cm. This corroborates a change in sediment lithology to non-layered, very fine–fine silty grey-coloured sediments in LU-II. Sediment grain-size increases around 506 cm and again around 483 cm clearly viewed by an increase in the Zr/K ratio and a peak in mean grain-size marking an increasing contribution of sand and coarser silts to the particle size distribution. Following a unit maximum in grain-size at 431 cm (5.1 μm) a decrease is observed with a value at 391 cm similar to the unit average of 3.82 μm. Grain-size then rises towards the LU-II/LU-I transition at 346 cm. Water content is significantly higher (average 51.8 %) and dry bulk density lower (average 0.87 g cm^{-3}) than in LU-III. MARs are generally lower than in LU-III, associated with lower
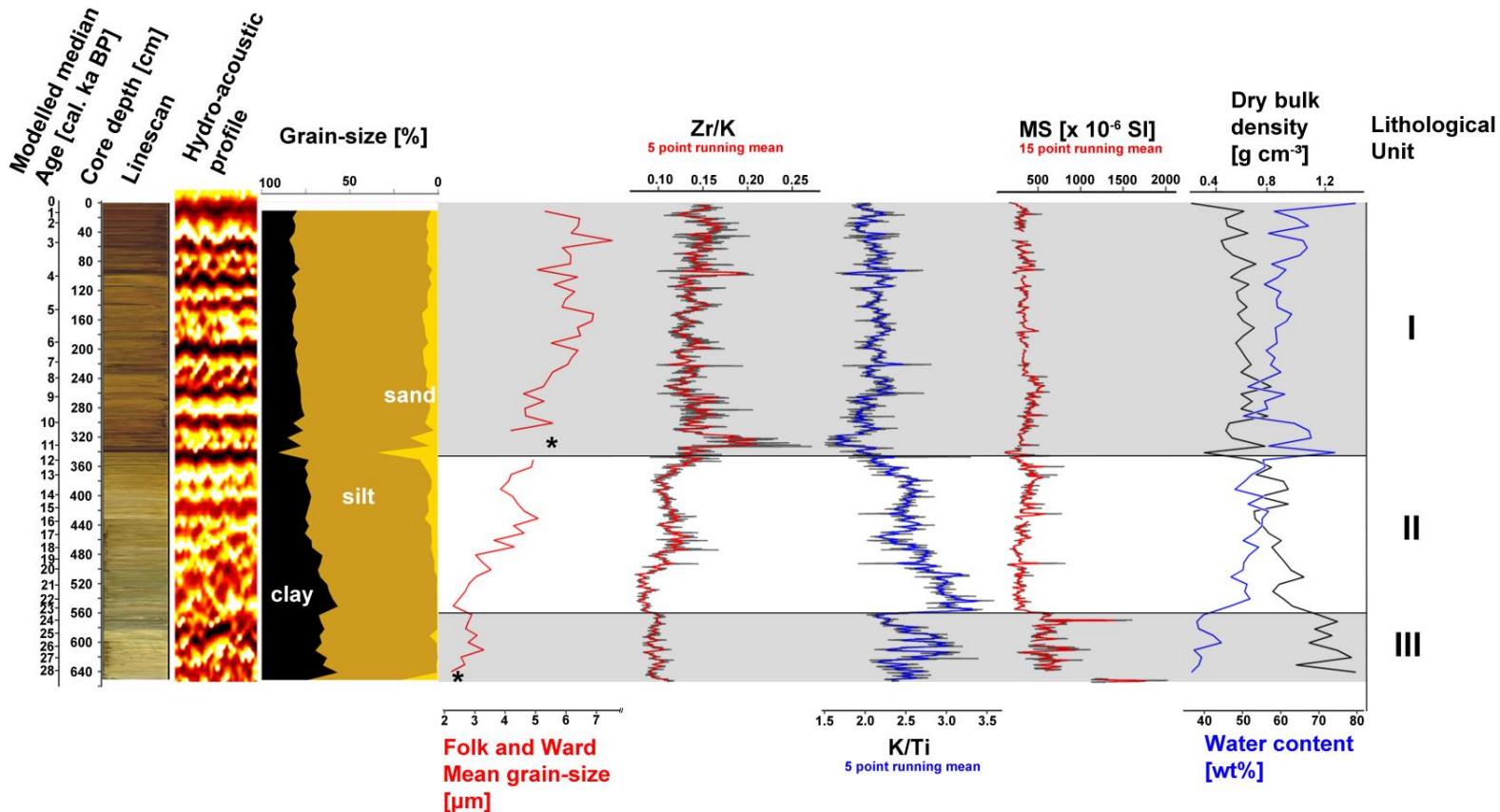

Figure 5. Sedimentological and sediment-geochemical proxies obtained from core EN18218 including measured grain-sizes, XRF grain-size proxies, magnetic susceptibility water content and dry bulk density alongside the hydroacoustic profile from the drilling location and lithological unit derivation (Grey-boxes). * in mean grain-size plot refers to three excluded data points (650.5, 341, 321 cm) of coarser mean grain-size (up to 25 μm).

uncertainty (average 0.017 g cm^{-2} a^{-1}, average 1σ uncertainty 0.013–0.019 g cm^{-2} a^{-1}) and follow variations in sedimentation rate with maxima at ca. 510.5 cm and 380–371 cm. TOC & TC values are significantly higher in LU-II (average TOC 0.77 %, average TC 0.78 %) and increase concomitantly to a maximum (> 2 % C) at the LU-II/LU-I transition in line with gradually darkening sediment colour and increasing Br/Al to brown coloured fine-silts at the top of the unit. The average OCAR in LU-II is more than double LU-III (average 1.32 g OC m^{-2} a^{-1}, average 1σ uncertainty 1.03–1.48 g OC m^{-2} a^{-1}) and rises from a minimum at 550 cm (0.72 g OC m^{-2} a^{-1}) to a unit maximum at 371 cm (2.67 g OC m^{-2} a^{-1}). TS shows higher values within LU-II (average TS 0.04 %) and increases in the upper part towards the LU-II/LU-I boundary at 346 cm. Nonetheless TS contributes very little to the total core biogeochemistry. The Mn/Fe ratio is more variable within LU-II and gradually increases from the LU-III/LU-II boundary upwards forming a plateau 472–363 cm before decreasing towards the LU-II/LU-I transition.

LU-I is typified by dark-coloured, fine-silt sediments of coarser grain-size than observed for all other units (average 6.5 μm) mirrored by Zr/K, Si/Al and K/Ti ratios. MARs achieve high values particularly between 311 and 251 cm and between 181.5 and 61.5 cm consistent with sedimentation rates (average 0.022 g cm^{-2} a^{-1}, 1σ uncertainty 0.015–0.028 g cm^{-2} a^{-1}). TOC & TC contents attain their highest values (average TOC 1.62 %, average TC 1.63 %) with a prominent maximum just after the LU-II/LU-I boundary (ca. 341 cm) and unit minimum (1.2 %) between 261 and 251 cm before increasing to values > 2 % at the modern sediment surface. Br/Al follows TOC and TC and increases slightly throughout the unit towards the sediment surface. TS demonstrates a broad peak between 371 and 271 cm commensurate with extremely low Mn/Fe ratio values. TS values then decrease and remain low with the exception of a maximum at the sediment-water interface. OCARs are significantly higher than in LU-II and LU-III, associated with higher uncertainty and vary between 1.56 to 6.3 g OC m^{-2} a^{-1} (average 3.53 g OC m^{-2} a^{-1}, average 1σ uncertainty 2.46–4.46 g OC m^{-2} a^{-1}) with values increasing across the LU-II/LU-I transition to high values between 311 and 271 cm generally consistent with higher TS and the Mn/Fe minimum. High OCARs are also observed between around 181.5 and 41.5 cm alongside high SRs and
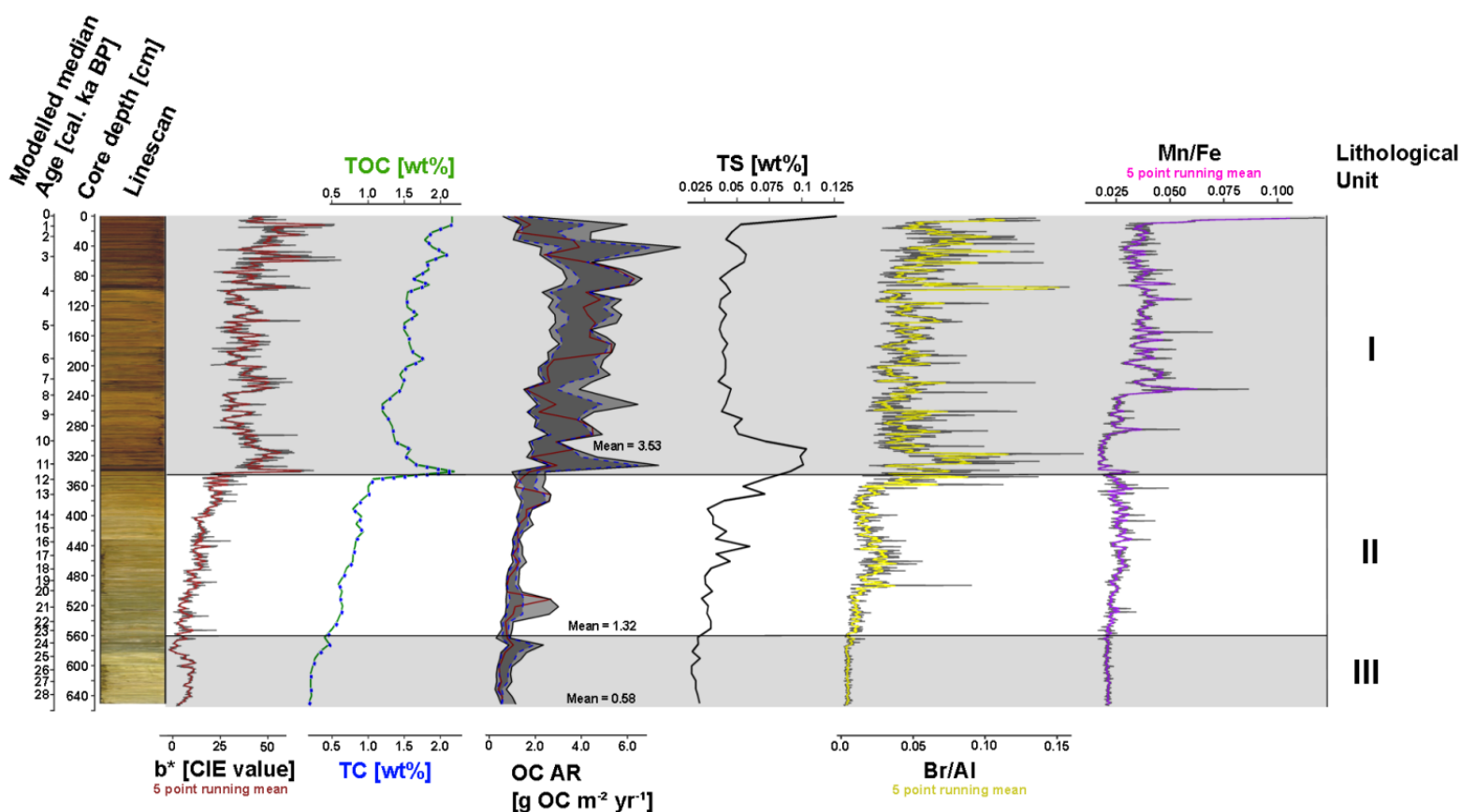
Figure 6. Biogeochemical proxies measured from samples obtained from core EN18218 (TOC, TC, TS) as well as from XRF (Br/Al, Mn/Fe) and line-scanning (b*). Average OCAR (Red line) is plotted alongside sigma uncertainty ranges (grey ribbons) synonymous with descriptions in Figure 4.

MARs in line with increasing TOC contents (maximum 6.3 g OC m^{-2} a^{-1}).

4.4 Lake carbon and sediment pools

Average sediment thicknesses and volumes are similar between both sediment packages but slightly greater within the LU-II/LU-III (AU2) package (Table 2). The total carbon pool (TOC$_{pool}$) calculated amounts to 0.26 ± 0.02 Mt with a respective average carbon density (TOC-density) of 7.85 ± 0.60 kg m^{-3}. LU-II & LU-III sediments at Lake Rauchuagytgyn displayed the lowest estimates with around 0.1 ± 0.007 Mt of carbon stored and a TOC-density of 5.65 ± 0.40 kg m^{-3} when compared with the more carbon rich LU-I sediments (TOC$_{pool}$ = 0.15 ± 0.005 Mt, TOC-density = 9.87 ± 0.34 kg m^{-3}). The total calculated sediment pool for total sediment mass deposited was estimated via bootstrapping as 25.7 ± 1.71 Mt with an average sediment density of 780 ± 52 kg m^{-3}. Individual calculation of sediment pools in LU-I and LU-II/LU-III yielded values of 9.33 ± 0.32 Mt and 17.1 ± 0.89 Mt respectively.

4.5 Results of principal component analysis

The PCA biplot (Fig. 7) of sedimentological, biogeochemical and accumulation rate data shows that PC1 (59.7 %) and PC2 (12.0 %) together explain 71.7 % of the total variance within the dataset. A clear division and clustering of data is observed that confirms the lithological unit definition and the main data trends described in sect. 4.2 & 4.3. The variance in the positive PC1 direction is controlled chiefly by productivity variables (TOC, TC, Br/Al, Br, TS, b*), grain-size (sand, silt, mean GS, Zr/K, Si/Al) and to a lesser degree sedimentation (SR) and accumulation rates of carbon (OCAR). Negative values of PC1 are explained by reduced organic content, increasing fine-grained contribution of clay, increased DBD, light colouration (l*) and MS, Ti, Ca, K and K/Ti. The mass accumulation rate controls chiefly variance within the PC2 direction (Fig. 7, Fig. S4).
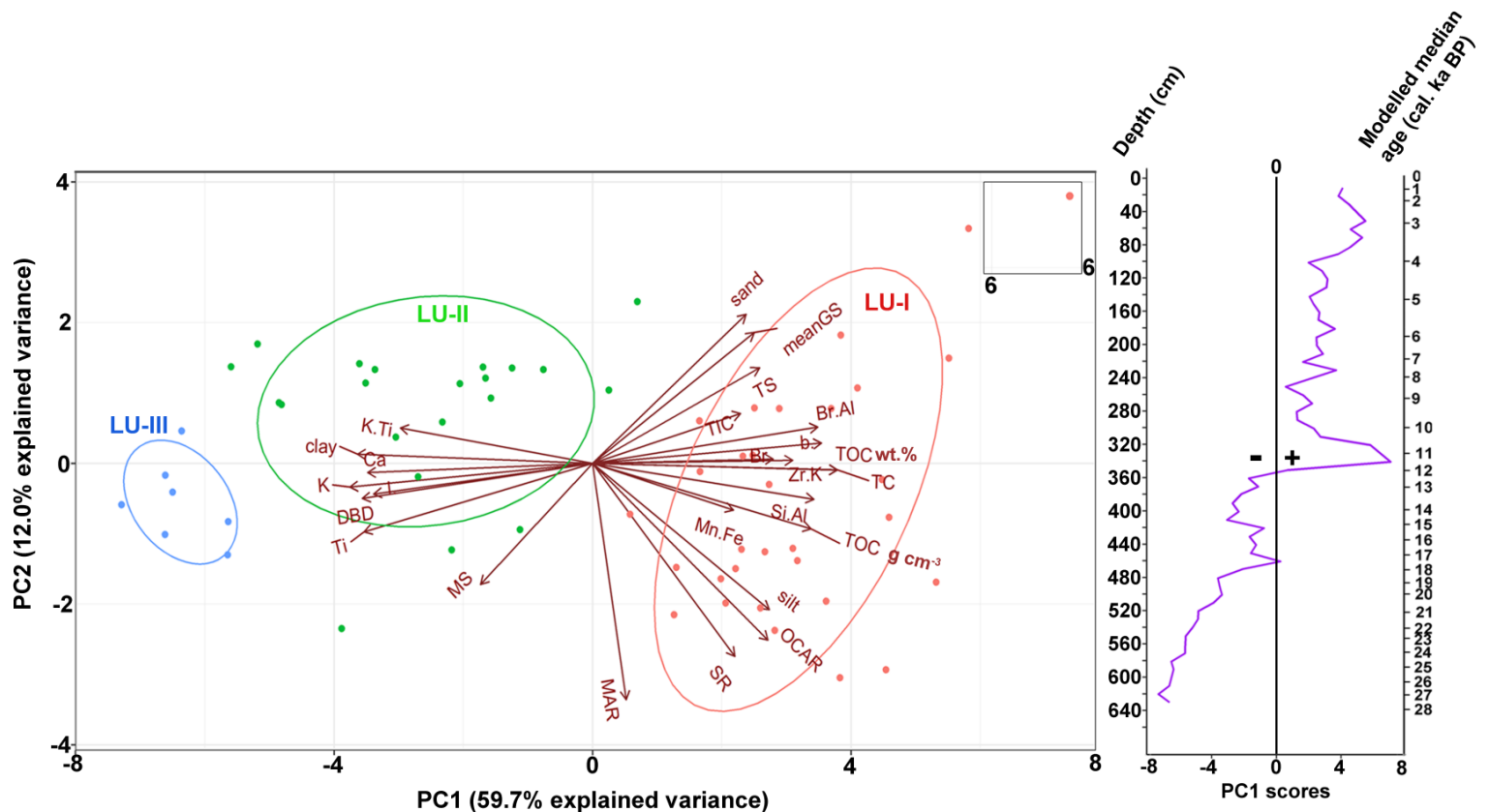
Figure 7. Principal component analysis biplot of sedimentological, biogeochemical and accumulation rate data from core EN18218. Samples are coloured and clustered according to their lithological unit definitions (LU-III, LU-II, LU-I). Also shown are the PC1 scores plotted stratigraphically in relation to depth and modelled age.

5. Discussion:

5.1 Accumulation history of Lake Rauchuagytgyn in a palaeoenvironmental context

5.1.1 Glacially influenced sediment and carbon accumulation during the early Marine Isotope Stage 2 (ca. 29–23.4 cal. ka BP)

400   Coarse sediments found directly at the base of core EN18218 consisting of pebble-sized clasts that prevented further core retrieval, alongside discontinuous and occasionally chaotic hydroacoustic reflectors within the lowermost portion of AU2, may suggest that the lake bottom substrate represents a diamicton that shares some similarities with basal sediments reported from other Arctic lake sites (cf. Finkenbinder et al., 2014). The presence of pebble-sized clasts, may imply that a lacustrine environment was either totally absent during
405   deposition of the basal sediment, or was dry for long periods of time. Basal structures observed within hydroacoustic data within the lower portion of AU2 may suggest a mixed origin of the coarse sediment that may be related to fluvial or possibly glacio-fluvial activity within the basin that subsequently influenced basin sediment distributions (cf. Lebas et al., 2019; Lebas et al., 2021). A lack of detailed sedimentological data of core base sediment, due to poor retrieval and limited penetration however limits the further comprehensive interpretation of
410   the lake bottom substrate within this study. Although radiocarbon ages show scatter throughout LU-III, a modelled core base age of around 29 cal. ka BP generally overlaps in timing with MIS2 recorded by other regional records and prominent Alaskan lake records (Asikainen et al., 2007; Finkenbinder et al., 2014; Vyse et al., 2020). Moreover, basal ages of several large northern latitude lakes, including dated basal diamicton from Harding Lake, Alaska show generally agreeable age overlap with coarse basal sediment preserved at Lake
415   Rauchuagytgyn (Anderson and Lozhkin, 2015; Brosius et al., 2021; Finkenbinder et al., 2014).

Overlying layered sediments pervasive throughout LU-III that are characterised by high magnetic susceptibility, dry bulk density and silty-clay composition may suggest the presence of a lake-proximal glacier and the concurrent deposition of minerogenic, predominantly fine-grained, glacially-derived suspended load to the lake basin within a glaciolacustrine setting (cf. Bakke et al., 2005; Gromig et al., 2019, Karlen and Matthews, 1992;
420   Leemann and Niessen, 1994b; Van der Bilt et al., 2015). This may be further supported by an abundance of the minerogenic elements Ca, Ti and K throughout LU-III, a light sediment colouration and very low organic content that suggest deposition of organic-poor, minerogenic material derived from a catchment glacier (Fig. 7). The fingerprint of minerogenic, glacially-derived suspended load sediment may plausibly be represented by strongly negative PC1 scores from principal component analysis clustered within LU-III of the PCA biplot (Fig. 7) (cf. Van
425   der Bilt et al., 2015). Catchment conditions during deposition of LU-III were likely cold with minimal within-lake and catchment vegetation productivity indicated across all biogeochemical proxies. Extremely low OCARs during the early MIS2 of ca. 0.58 g OC m^{-2} a^{-1} suggest minimal organic carbon input to the basin sediment that was predominantly autochthonous in origin with very limited contribution from catchment vegetation (Kokorowski et al., 2008a). Lacustrine palynological records and vegetation reconstructions of the catchment surrounding Lake
430   Ilirney (ca. 50 km south) during MIS2 agrees well with cold conditions with low pollen productivity of catchment flora represented by low pollen concentrations (Andreev et al., 2021). In addition, pollen reconstructed July temperatures were 4–5 °C lower than modern in agreement with unfavourable climate conditions for organic carbon productivity (Andreev et al., 2021). Sedimentological records from Lake Ilirney during MIS2 also agree with extremely low within-lake productivity represented by very low TC and absent diatoms (Vyse et al., 2020).
435   Preliminary diatom analyses also show a complete absence of diatoms within LU-III in line with cold and possibly

turbid water conditions (Biskaborn, unpublished data; Finkenbinder et al., 2014). Organic material arriving at the sediment-water interface was likely preserved by low oxygen conditions. This is recorded by low and stable values of the XRF-derived Mn/Fe ratio that well represents the redox conditions at the sediment-water interface (cf. Baumer et al., 2020; Biskaborn et al., 2019; Fritz et al., 2018; Heinecke et al., 2017; Naeher et al., 2013; Píšková et al., 2019).

Finer grain-sizes directly measured by laser diffraction are supported by indirect, XRF-derived grain-size proxies for finer, clay-dominated sediment (K/Ti) and of coarser sediment (Zr/K, Si/Al). Fine-grained composition likely reflects deposition beneath a quasi-permanent lake ice layer that further reduced within-lake productivity through limiting light penetration with insufficient irradiance required by algal communities and hence diminishing organic matter export to the hypolimnion (Andersen et al. 1993; Bouchard et al., 2011; Croudace & Rothwell., 2015; Cuven et al., 2010; Mclaren & Bowles. 1985). Thus, during deposition of minerogenic sediment within LU-III the lake may have been of cold-monomict type (Cremer and Wagner, 2003). Sediment input at Lake Rauchuagytgyn was generally low during LU-III deposition as represented by comparatively low SRs and MARs and was likely temporally continuous, with no evidence of unconformities found within sedimentological data. The uncertainty in the positive sigma direction may suggest that rates could be higher when integrating uncertainty associated with age inversions within LU-III. Sedimentation rates reported for Lake El´gygytgyn crater lake (Fig. 1) were low during MIS2 (4.8 cm/ka), compared to higher rates (7.6 cm/ka) during the Holocene (Nowaczyk et al., 2007). A similar finding was made for Harding Lake in Alaska whereby sedimentation rates during the Last Glacial Maximum (30.7 to 15.7 ka) were generally < 0.1 mm/yr but temporally continuous throughout deposition (Finkenbinder et al., 2014). In both of these settings, low sedimentation rates were interpreted as a consequence of thick, quasi-permanent lake surface ice cover and an extremely thin or absent catchment tundra active layer during cold episodes that reduced catchment sediment delivery and wind-driven sediment redistribution (Asikainen et al., 2007; Francke et al., 2013; Melles et al., 2007). Moreover, a similar observation at lake Karakul, Tajikistan of lower sedimentation rates during MIS2 since ca. 29 cal. ka BP (0.15 mm a-1) when compared with Holocene sedimentation rates (0.84 mm a−1) was also explained by reduced sediment input during MIS2 compared to the Holocene alongside reduced organic matter accumulation (Heinecke et al., 2017). The low sedimentation and mass accumulation rates at Lake Rauchuagytgyn during the early MIS2 and the Late Glacial may be supported by the generally equitable thicknesses and sediment volumes between the AU2 (LU-II/LU-III) and AU1 (LU-I) sediment packages derived hydroacoustically (Table 2). Differences are however observed when MIS2 accumulation rates are compared with other Siberian glacial lake sites including Lake Bolshoye Shchuchye in the Ural Mountains (average Last Glacial Maximum (LGM) 1.68 mm a^{-1}). Lake Bolshoye Shchuchye demonstrates a voluminous LGM sediment package (0.325 km^3) six times the volume of the Holocene sediment package (0.05 km^3) which shows markedly lower sedimentation rates (0.36 mm a^{-1}) and is interpreted to result from intense glacial erosion of the catchment during the LGM (Haflidason et al., 2019).

The difference in glacial sediment accumulation between sites may relate to multiple, interacting factors including the duration of lake surface ice cover, the thickness of the catchment active layer, the existence/absence of deep-water conditions and also differences in glacier dynamics between catchments (Asikainen et al., 2007; Francke et al., 2013). Remote sensing based studies of Chukotkan glacial geomorphology and structures within the Rauchua valley have suggested the presence of a passive catchment glacier, ca. 25 km in length that extended along the length of the Rauchua river valley and discharged into the Rauchuagytgyn basin during marine isotope stage 2 (Glushkova, 2011). Thus, the catchment glacier may have been predominantly non-erosive during the early MIS2 and hence not contributed significant sediment volume to the lake basin supporting

the low rates of sediment and mass accumulation discussed here (Gurnell et al., 1996). It must be however noted that the radiocarbon age scatter in LU-III contributes uncertainty regarding sediment age and hence the SRs and MARs derived for this interval as marked by the wider uncertainty band within the presented age model (Fig. 4b). Such age scatter may be in part associated with catchment glacial activity that could have led to the reworking of older catchment organic containing sediments with subsequent deposition within the glaciolacustrine environment (cf. Lunkka et al., 2001). The usage of bulk sediment radiocarbon dating may additionally exacerbate this problem and add to radiocarbon uncertainty within LU-III as noted by Oswald et al. 2005 and others regarding dating of organic poor, Last Glacial Maximum lacustrine sediments in Alaska and Siberia. Furthermore, the presence of layering within LU-III, may also indicate potentially higher sedimentation rates across the unit (cf. Leemann and Niessen, 1994b). The lack of absolute dating of glacial structures within the Rauchua valley by Glushkova, 2011, adds additional uncertainty regarding the temporal dynamics of the catchment glacier.

The temporally continuous, fine-grained, minerogenic sediment accumulation preserved within LU-III can likely be attributed regionally to the MIS2 "Sartan" glaciation recorded within Chukotka (Anderson & Lozhkin 2015; Brigham-Grette et al., 2003; Melles et al., 2012; Vyse et al., 2020) and the Itkillik II glaciation in Alaska, eastern Beringia (Hamilton and Ashley, 1993). Glaciation during this time was associated with asynchronous but early glacial advances in Alaskan mountain ranges between 31 and 28 cal. ka BP and advances in western Beringian glaciers to maximum extents between 27 and 20 cal. ka BP (Brigham-Grette et al., 2003; Elias and Brigham-Grette, 2013 and references therein). The presence of a valley glacier at Lake Rauchuagytgyn is in contrast to more westerly, eastern Russia sites from the Verkhoyansk mountains where no glacial activity was witnessed during MIS2 (Diekmann et al., 2017; Stauch and Lehmkuhl, 2010). This supports previous suggestions that despite cold conditions, higher moisture derived from the Pacific Ocean permitted the existence of glaciers within Chukotka (Stauch and Gualtieri, 2008).

5.1.2 Mid MIS2-early MIS1 accumulation during progressive climate amelioration (ca. 23.4–11.69 cal. ka BP)

Sediment accumulation recorded by LU-II sediments represents a transitional mode between the early MIS2 and Holocene clearly viewed within PCA results between ca. 23.4 and 11.69 cal. ka BP and likely reflects a time-progressive shift towards the early stages of paraglacial deposition (Fig. 7). Hydroacoustic data show an upward transition to stable, deep water, lacustrine deposition represented by the increasing prevalence of stronger amplitudes from well-stratified reflectors (cf. Lebas et al., 2021; Haflidason et al., 2019). A clay maximum and grain size minimum at ca. 550 cm (ca. 22.7 cal. ka BP) may suggest initial increases in lake water-depth through glacial melt additions that could have led to the observed reduced SRs and MARs at this time. This may be supported by the high values of K/Ti (clay contribution) and low values of Zr/K and Si/Al (proxies for coarser grain-sizes) (Kilian et al., 2013; Křibek et al., 2017; Cuven et al., 2010). It is also likely that the persistence of the quasi-permanent ice layer continued to contribute to predominantly fine-grained, low energy deposition (Asikainen et al., 2007). The strong increase in Zr/K accompanied by increased sand and silt contribution firstly at ca. 20.5 cal. ka BP consistent with a dramatic peak in SR and MAR values and again ca. 18.5 cal. ka BP likely reflects increasingly rapid glacial retreat (Gromig et al., 2019). The timing of these system responses is generally consistent with depositional changes recorded at Lake Ilirney in response to deglaciation ca. 20 ka (Vyse et al., 2020) and those proposed for Alaskan glacial retreat interpreted from dated moraine deposits and lacustrine sediments (20–19 ka BP)(Elias and Brigham-Grette, 2013; Finkenbinder et al., 2015 and references therein). Progressive deglaciation facilitated the gradual opening of the lake catchment area and development of fluvial

systems that plausibly enhanced sediment load and input to the lake basin through the initiation of paraglacial processes (Ballantyne, 2002; Dedkov, 2004). Sediment dynamics were likely controlled by inflowing rivers at the lakes southern margin as indicated by the greatest thicknesses of sediment within the southern sub-basin deposited within AU2 (Fig. 3c). Thick sediments within AU2 in the northern sub-basin may indicate additionally enhanced sedimentation derived from the north. The occurrence of a rhomboidal-shaped deposit similar to preserved lake sediments within other lacustrine and continental shelf environments at the northern shelf-northern sub-basin transition may represent a mass transport deposit during some part of AU2 deposition (Fig. 2b, Fig. S5) (Baster et al., 2003). Catchment sediment availability likely also began to increase during this time due to gradual sub-aerial exposure of subglacial sediments that subsequently became entrained within paraglacial river systems or transported to the lake via aeolian processes contributing to progressively increasing sedimentation rates (Tripathi & Rajamani, 1999; Wang et al., 2015).

Organic carbon accumulation rates at the base of LU-II were slightly higher than LU-III signifying increasing organic carbon production and accumulation across the LU-III/LU-II transition. Subsequently increasing rates alongside up-core sediment darkening and increases in all organic proxies across LU-II points towards continuous growth in carbon accumulation related to ameliorating conditions during the Mid MIS2-early MIS1 onwards. Organic productivity was most likely dominated by autochthonous productivity from within-lake algae with only minor contributions from catchment vegetation. Though nitrogen was not measured as part of this study, extremely low TOC/TN ratios measured for sediments at the nearby glacial Lake Ilirney during the Late Glacial implied that most organic matter was derived from protein rich algal sources and not from cellulose-rich and protein-poor vascular land plants from the lake catchment and from macrophytes within the lake (Baumer et al., 2020; Meyers & Teranes., 2005; Vyse et al., 2020). This is supported by low pollen concentrations recorded within the Lake Ilirney pollen record and the persistence of *Poaceae* and *Artemisia* during the Late Glacial that signify persistently cold conditions and low catchment pollen productivity (Andreev et al., 2021). Based on the similarities between the lakes and their catchments, their proximity, and a lack of macrophytes at both sites, a similar interpretation can be postulated for Lake Rauchuagytgyn (Sifeddine et al., 2011). Higher and more variable Mn/Fe ratio values throughout much of LU-II point towards increased oxygen at the sediment-water interface that could have enhanced degradation of organic matter (Baumer et al., 2020; Fritz et al., 2018). This could be indicative of a gradually increasing summer open water season with more intensive mixing of the water column through wind and also through enhanced fluvial inflow during progressive Late Glacial climate amelioration (Baumer et al., 2020).

A reduction in accumulation rates ca. 12.6 to ca. 11.69 cal. ka BP, broadly associated with a small reduction in sediment mean grain-size may represent some evidence of reduced accumulation due to cooling associated with the Younger Dryas (YD). The magnitude of this is however not substantial when all proxies are considered together within principal component analysis (Fig. 7). Moreover, missing evidence of younger moraines from the catchment implies that there was no glacial re-advance (Glushkova, 2011). These findings may be consistent with recent regional and trans-regional records that suggest a spatially variable Younger Dryas climatic event in East & Far East Russia and parts of Eastern Beringia (Anderson & Lozhkin, 2015; Finkenbinder et al., 2015; Kokorowski et al., 2008b; Lozhkin & Anderson, 2013; Lozhkin et al., 2018). The lack of significant evidence for a strong Younger Dryas climatic event may also partially reflect seasonal differences in the sensitivity of physical and geochemical proxies to climatic or environmental change, as has been discussed in studies of sediment cores from Burial Lake, Alaska (Finkenbinder et al., 2015).

5.1.3 Holocene controls on basin sediment and carbon dynamics (ca. 11.69 cal. ka BP–present)

The Holocene start is marked across all proxies by increasing organic proxy values and sediment grain-size across the LU-II/LU-I boundary (11.69 cal. ka BP) alongside increasing accumulation rate values (Figs 5, 6, 7). High TOC and TS and a dark sediment colour form a prominent peak during the early Holocene between ca. 11.5 and 9.7 cal. ka BP synchronous with the lowest values of Mn/Fe that could reflect increased preservation of organic material under low-oxygen conditions at the sediment-water interface alongside enhanced organic productivity (Fig. 6) (Fritz et al., 2018). Increasing carbon accumulation is supported by rising organic carbon accumulation rates that demonstrate high early Holocene values between ca. 10.2 and 9.2 cal. ka BP. Low K/Ti values during the early Holocene that subsequently persist throughout the mid-late Holocene may reflect increased chemical relative to physical weathering due to the leaching of K from clastic material entering the lake by enhanced catchment pedogenic processes that influenced OCAR values as well as responding to coarser Holocene grain-sizes (Baumer et al., 2020; D'Arcy & Carignan, 1997). The timing of this phase agrees well with the timing of warm and humid environments interpreted during the early Holocene recorded at Lake Emanda, central Yakutia (11.5–9.0 cal. ka BP) and coincides with the maximum in local solar insolation (Baumer et al., 2020; Berger & Loutre 1991). Moreover, this finding is consistent with palynological records from Lake Ilirney and from a Holocene short core from Lake Rauchuagytgyn which show evidence for a local Holocene thermal maximum ca. 10.6–7 cal. ka BP (Andreev et al., 2021).

Increasing early Holocene sediment and mass accumulation rates alongside greater sand contribution may relate to the input of coarser grained fluvial detrital material from a paraglacial, deglaciated catchment and could result from a water budget change associated with warmer and more humid conditions (Ballantyne, 2002). This is supported by increasing Zr/K and Si/Al ratio values during the early Holocene that support coarser grain sizes that may relate to enhanced input of coarser silts and sands (cf. Píšková et al., 2019). It must however be noted, that higher Si/Al ratio values may also additionally reflect abundant diatoms within Holocene sediments (Procházka et al., 2019). Annual precipitation (P_{ann}) reconstructed from palynological records at Lake Ilirney suggested an increase from ca. 225 mm during the Late Glacial to ca. 300 mm in the early Holocene that could have enhanced catchment surface runoff and hence fluvially driven reworking of unstable-metastable glacially deposited sediment by paraglacial processes (Andreev et al., 2021; Ballantyne, 2002). Heinecke et al. (2017) proposed a similar scenario to explain increased Holocene sedimentation rates and increased grain-sizes during the end of the Late Glacial and early Holocene (13.3–6.6 cal. ka BP) at glacial Lake Karakul. Moisture in north-eastern Siberia during interglacials, is derived mostly from warm North Atlantic surface waters and brought via the westerlies to the region (Melles et al., 2007). The waning of the Scandinavian and Barents-Kara ice-sheets likely allowed the passage of moister westerlies to the region that were blocked during the Last Glacial Maximum (Elias & Brigham-Grette 2013; Meyer et al., 2002). Increased sedimentation rates also additionally enhanced carbon burial and preservation (Einsele et al., 2001). Enhanced precipitation and fluvial input to Lake Rauchuagytgyn during the early Holocene could have led to lake level increase and deep lacustrine conditions at the core location that restricted mixing of the water column, leading to stratification and may provide a possible explanation for low oxygen conditions (cf. Baumer et al., 2020). An increase in precipitation and rising lake levels was also interpreted for early Holocene sediments preserved at Harding Lake, Alaska (Finkenbinder et al., 2014). Deep lacustrine conditions alongside enhanced early Holocene within-lake and catchment productivity thus likely led to enhanced carbon deposition and preservation at Lake Rauchuagytgyn.

600 A decrease in TOC content (wt%) to a minimum at ca. 8.6 cal. ka BP along with decreasing organic carbon and sediment and mass accumulation rates from 8.9 cal. ka BP to a minimum at ca. 7.7 cal. ka BP alongside finer grain-sizes may reflect some local environmental change and is generally consistent with a Holocene T_{July} minimum at 7.8 cal. ka BP and P_{ann} minimum at 7.6 cal. ka BP recorded within a Lake Rauchuagytgyn short core (Andreev et al., 2021). This may possibly be associated with cooling associated generally with the 8.2 cal. ka BP

605 event recorded at other locations within Siberia (Biskaborn et al., 2016). A degree of similarity between the TOC trend following the early Holocene at both Lake Rauchuagytgyn and Lake Emanda may also suggest that bacterial sulphate reduction contributed to the reduced sedimentary organic carbon content during this interval (Fig. 6) (Baumer et al., 2020). A subsequent increase in OCARs from ca. 6.1 cal. ka BP consistent with progressively increasing TOC values towards the modern lake sediment surface represents increased

610 accumulation of organic carbon consistent with increasing mean July temperatures (T_{July}) to a maximum ca. 13.3 °C during the mid-late Holocene by ca. 4.6 cal. ka BP (Andreev et al., 2021). Synchronous increases in SR and MAR along with coarser grain-sizes may reflect extended periods of ice-free lake surface conditions during summer associated with high T_{July} (Fig. 4,5) (Finkenbinder et al., 2014). Extended open water conditions during this time and throughout the Holocene likely led to longer phases of summer catchment aeolian input, as well as

615 increased wind-driven shoreline erosion and sediment redistribution due to the impact of summer storms (Asikainen et al., 2007; Francke et al., 2013; Vologina et al., 2003). This hypothesis is supported by the highest Mn/Fe ratio values for the core, supportive of enhanced wind and fluvial driven lake mixing processes and weaker stratification (Doran, 1993; Baumer et al., 2020; Regnéll et al., 2019). Francke et al. 2013 argued that coarser grain-sizes and enhanced sedimentation at Lake El´gygytgyn during Interglacials was controlled by

620 summer temperatures affecting lake ice cover and hence aeolian input, wind-driven sediment redistribution as well as catchment active layer thicknesses and water availability and was not affected by lake-level variations.

Decreasing accumulation rates from ca. 3.6 cal. ka BP to present could reflect reduced late-Holocene sediment input due to neoglacial cooling and is in line with variable T_{july} and low P_{ann} recorded within the Ilirney and Rauchuagytgyn short core records and generally lower late Holocene Mn/Fe ratio values (Fig. 6) (Andreev et al.,

625 2021). This could tentatively be interpreted to represent a shortening of the summer open water season.

Enhanced fluvial input to the lake basin throughout the Holocene from the Rauchua river valley and from the south-east lake margin are reflected in hydroacoustic and interpolated sediment thickness data (Fig. 3b) from AU1 which show greater thicknesses within the southern sub-basin. A similar distribution has been observed at glacial lakes Bolshoye Shchuchye & Levinson-Lessing (Haflidason et al., 2019; Lebas et al., 2019). The presence

630 of an alluvial fan ca. 600 m in diameter at the south-eastern margin is supportive of intensified Holocene paraglacial processes that resulted in an input source of coarser fluvial and alluvial detrital material into the southern sub-basin contributing to the observed increased sedimentation and mass accumulation rates (cf. Doran, 1993; Smith and Jol, 1997). This is further supported by coarse, sand-dominated surface sediments close to the alluvial fan front (site EN18220) (Fig. 1 & Figs S6, S7). Modern observations at Lake El´gygytgyn have

635 shown that summer fluvial activation associated with snowmelt can lead to significant deposition of coarse material of cobble-grade material to the lake basin (Nolan and Brigham-Grette, 2007). Heightened availability of catchment sediment material due to thicker catchment active layer thicknesses during the Holocene may also provide an additional sediment source leading to increased sedimentation. A thick tundra active layer present during the Holocene at Lake El´gygytgyn was suggested to have contributed to greater detrital input to the basin

640 as well as promoting the weathering of clay minerals (Asikainen et al., 2007; Francke et al., 2013). This further supports the low K/Ti ratios during the Holocene that evidence intensified chemical weathering (Regnéll et al.,

2019). Acoustic reflectors preserved within AU1 generally reflect well-developed lacustrine deposition under deep-water conditions prevalent across the basin (Fig. 2)(Lebas et al., 2019). Some variability is observed within hydroacoustic data at the northern shelf where sediments are thin and evidence of erosion of sediments are seen (Fig. S2). This likely represents low deposition due to sediment transport into the deeper basin and feasibly some Holocene lake-level variability of several metres permitting localised erosion into shallow areas (Moernaut et al., 2010).

5.2 Comparisons of carbon and sediment dynamics on a trans-regional scale

5.2.1 Organic Carbon Accumulation Rates (OCARs)

The calculated organic carbon accumulation rates for Lake Rauchuagytgyn represent the first calculated values for an Arctic Siberian glacial lake. As such, limited comparable studies exist and are restricted to studies of Siberian thermokarst lake systems that are generally younger and smaller (Anthony et al., 2014) and to the much larger Lake Baikal (Martin et al., 1998). Comparisons must therefore be additionally drawn to boreal and glacial lakes from North America and northern Europe, as well as to proglacial and bedrock-catchment lakes from Greenland. Significant differences however exist between these lake systems relating to contrasting environmental conditions prevailing at different latitudes as well as high variability with regards to lake and catchment spatial extent, lake water depth and catchment environmental and vegetation properties.

The overall Holocene average organic carbon accumulation rate of 3.53 g OC $m^{-2} a^{-1}$ for Lake Rauchuagytgn is significantly higher than those reported for the Pleistocene units represented by LU-II & LU-III (AU2) of 1.08 g OC $m^{-2} a^{-1}$ (Figs. 8, 9a). This is in accord to increased organic productivity, carbon accumulation and generally higher SRs and MARs during the Holocene. The calculated Holocene rate is very similar to that obtained for Holocene deposits of boreal lakes from northern Quebec, Canada (mean 3.8 g OC $m^{-2} a^{-1}$) that were also studied using an equivocal hydroacoustic approach to account for sediment focussing and to rates obtained for Lake Baikal (mean 2.8 g OC $m^{-2} a^{-1}$) (Ferland et al., 2012; Ferland et al., 2014; Martin et al., 1998) (Figs. 8, 9a). The range of Holocene rates is on average lower but generally overlaps with Holocene organic carbon accumulation rates of small (0.033- 0.73 km^2) Greenlandic lakes (mean 6 g OC $m^{-2} a^{-1}$) (Anderson et al., 2009), and to small (0.022- 0.145 km^2) Uinta glacial lakes, USA (mean 5.4 g OC $m^{-2} a^{-1}$) (Munroe & Brencher, 2019). A strong resemblance is also observed when comparing to rates of accumulation calculated for Finnish boreal lakes that became ice free at the Holocene start (Figs 8, 9a, 9b) (Pajunen, 2000; Kortelainen et al. 2004). The average Holocene and whole core Rauchuagytgyn rates plot well within the range of Finnish lakes and close to the mean of shallow Quebec boreal lakes when considering sediment volumes derived from sub-bottom profiling approaches or estimated from core length and lake surface area (Uinta lakes) (Fig. 9a). Recent syntheses of average carbon accumulation rates within European lakes also suggest similar mean accumulation rates ca. 5.6 g OC $m^{-2} a^{-1}$ (Kastowski et al., 2011).

675 Pronounced differences exist when compared with larger lake systems reported from Alberta, Canada (mean 15 g OC m^{-2} a^{-1}) (Campbell et al., 2000) and global lakes, reservoirs and peatlands (Dean & Gorham, 1998; Mendonça et al., 2017). Furthermore, average Holocene rates calculated for thermokarst lakes from the Cherskii-Kolyma Tundra, Far East Siberia are markedly higher (mean 47 g OC m^{-2} a^{-1}) than Rauchuagytgyn rates (Anthony et al., 2014)(Fig. 8).
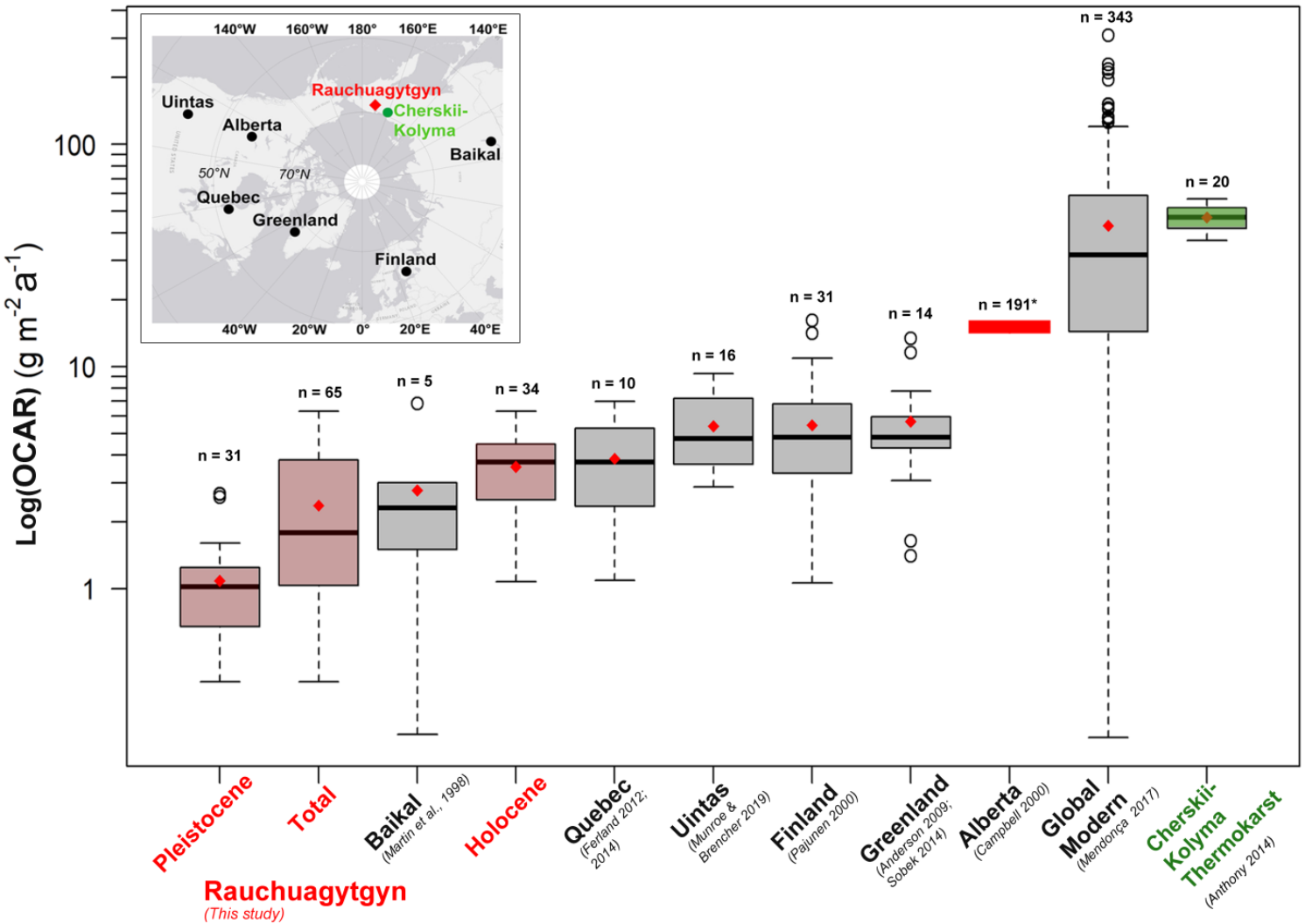
Figure 8. Comparison Log-boxplot of average organic carbon accumulation rates (OCARs) for Lake Rauchuagytgyn with carbon accumulation rates from other regions. Rauchuagytgyn OCARs include a total of 65 downcore points and plot close to boreal lake sites and to Lake Baikal (ESRI 2020). The global modern dataset of Mendonça et al., 2017 included OCARs from 343 globally distributed lake sites (see Text S1). Only the average OCAR across Alberta lakes was provided in Campbell et al. 2000 and hence the average is displayed as a red bar. Study references are quoted below the study regions.

680

5.2.2 Sediment and carbon pools within a Siberian Arctic glacial lake basin

The total sediment pool of Rauchuagytgyn was estimated to 25.7 ± 1.71 Mt within a sediment volume of ca. 0.033 km^3, with an average dry bulk sediment density of 780 kg m^{-3} (0.780 g cm^{-3}). The sediment at Lake Rauchuagytgyn is predominantly inorganic as represented clearly by the very low total organic carbon content of

685 sediments. The average calculated sediment density shows high agreement with global syntheses of sediment bulk density measured from lacustrine and fluvial sediments (Avnimelech et al., 2001; Haflidason et al., 2019; Munroe & Brencher, 2019; Sekellick et al., 2013). Sediment densities are however observed to be significantly

higher than the average calculated for Holocene Finnish lakes (0.25 g cm^{-3}) mostly due to greater organic carbon and water contents than those remarked for Rauchuagytgyn sediments (Pajunen, 2000).

690   The estimated TOC$_{pools}$ (total ca. 0.26 Mt) and TOC-densities (total ca. 7.85 kg m^{-3}) of Lake Rauchuagytgyn sediments presented here, represent the first assessment of carbon pools within a Siberian Arctic glacial lake. Our results show that the sediment TOC$_{pool}$ and TOC-density is relatively small, particularly during the deposition of LU-III and LU-II that covers the late Pleistocene and is in agreement with low OCARs discussed in sect. 5.2.1. The small carbon pool is especially evident when compared with carbon budgets and sediment volumes reported

695   for Pleistocene-Holocene age yedoma and thermokarst and drained thermokarst lake basin records (DTLB) from Alaska, as well as Holocene TOC$_{pools}$ and sediment volumes of Alberta glacial lakes, Canada (Fig. 9b) (Campbell et al., 2000; Jongejans et al., 2018). Pleistocene-Holocene sediments obtained from thermokarst lagoon and permafrost sediments from the Bykovsky Peninusla, northern Yakutia also show significantly higher estimated TOC$_{pools}$ (Bykovsky lagoons 5.72 Mt) and TOC-densities (mean 15.29 kg m^{-3}) relative to their small spatial

700   extents (Jenrich et al., accepted; Schirrmeister et al., 2011). Resemblance is however observed between the TOC$_{pools}$ (0.23 Mt) and TOC-densities (12.54 kg m^{-3}) of Polar Fox thermokarst lagoon (Bykovsky) and
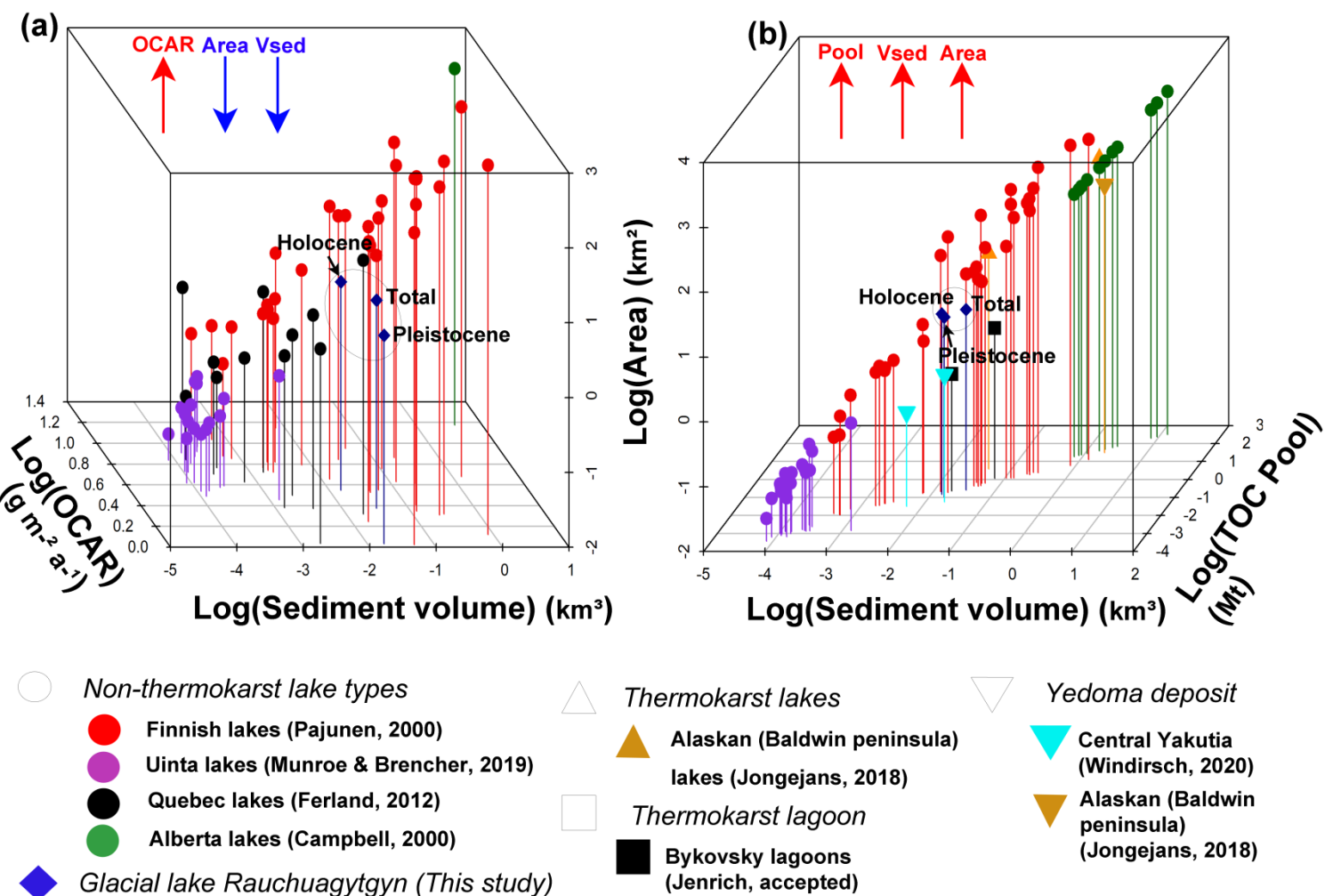
Figure 9. (a) 3D log scatter plot of organic carbon accumulation rate (OCAR) vs lake sediment volumes and surface areas. The average carbon accumulation rate for the Holocene at Lake Rauchuagytgyn closely resembles that of Holocene-age Finnish and Quebec lakes and generally lies on a trajectory of increasing OCAR with decreasing sediment volume and area. **(b)** 3D log scatter plot of Carbon pool vs sediment volume and area. The Rauchuagytgyn data-points are highlighted with ellipses in both plots. Rauchuagytgyn displays similar carbon pools to Finnish lakes, Bykovsky thermokarst lagoons and Central Yakutian yedoma deposits. Rauchuagytgyn sediments possess however significantly lower carbon pools relative to volume and area than Alaskan (Baldwin Peninsula) thermokarst lake and yedoma deposits and Alberta lakes.

Rauchuagytgyn particularly within Holocene sediment of LU-I (TOC$_{pool}$ 0.15 Mt, TOC-density 9.87 kg m^{-3}) (Jenrich et al., accepted). Moreover, similar values of TOC$_{pools}$ and TOC-density relative to sediment volume have been estimated for Pleistocene–Holocene yedoma and alas sediments from central Yakutia, eastern Russia (yedoma: 0.057 Mt, 5.27 kg m^{-3}, alas: 0.032 Mt, 6.07 kg m^{-3}) that are closer to the range of the Pleistocene values calculated at Rauchuagytgyn (0.1 Mt, 5.65 kg m^{-3}) (Windirsch et al., 2020). The highest degree of similarity is achieved with comparisons of TOC$_{pools}$, surface areas and sediment volumes to Finnish lakes whereby Lake Rauchuagytgyn pools lie on a distinct trend in 3D logarithmic space within the range and around the mean of Finnish lakes (Fig. 9b) (Pajunen et al., 2000; Kortelainen et al. 2004). Estimated carbon pools from Uinta glacial lakes show markedly lower values that show they store significantly less carbon within their smaller sediment volume (Munroe and Brencher, 2019).

5.2.3 Regional and local controls on carbon accumulation and methodological limitations

Lake Rauchuagytgyn stores predominantly inorganic sediment detritus and demonstrates carbon dynamics not strongly dissimilar from other high-latitude lake systems. Differences are however revealed when comparisons of carbon dynamics are made to thermokarst and drained thermokarst lakes (DTLB), large Alberta glacial lakes and global lakes in general. The interplay between many, varied factors likely contribute to major differences in carbon accumulation dynamics between different deposits and regions that are beyond a major discussion here and have been broadly considered elsewhere (Ferland et al., 2012; Kastowski et al., 2011; Sobek et al., 2009). Carbon accumulation at Lake Rauchuagytgyn is however likely affected by several key factors that can be identified.

Its mountainous, high-latitude, tundra location represents cold and dry environmental conditions that provide a first order climatic limit on catchment and lake internal primary productivity and hence carbon production. The expression of a cold climate is marked by open herb- and graminoid tundra vegetation dominated by *Poaceae* and *Dryas octopetala* L. with the absence of vegetation at higher altitudes on lake proximal slopes and within the mountainous lake catchment (Shevtsova et al., 2020). The occurrence of a well-developed lake surface ice-layer up to ca. 1.8 m in thickness that is present for ca. 9 months additionally contributes to reduced rates of algal primary productivity by limiting the availability of light as well as the allochthonous input of particulate (POC) and dissolved organic carbon (DOC) via fluvial and/or aeolian pathways (Baron et al., 1991; Nolan et al., 2002; Woolway & Merchant, 2019). An additional contributing factor to reduced catchment carbon export to Lake Rauchuagytgyn is likely connected to the steep, mountainous topography and poor soil development within the lake catchment. Catchment soil development is limited primarily to thin cryosols but large areas of barren land exist at higher altitudes (Bünseler, 2019; Shevtsova et al., 2020). D´Arcy and Carignan (1997) suggested that lakes situated in steep catchments with thin soils demonstrate low DOC exports to lake systems that may lead to reduced carbon loading and hence reduced carbon accumulation. Low modern carbon export and production is supported by the extremely low DOC contents of lake surface water samples at Lake Rauchuagytgyn (Table S1) and at other regional lake sites (Huang et al., 2020) that support low organic matter export from the catchment (Bouchard et al., 2016). These factors were plausibly enhanced under more strongly continental, colder and drier Pleistocene climatic conditions that led to extremely low OCARs and a small carbon pool as evidenced by the multiple environmental proxies discussed throughout sect. 5.1 (Fig. 9)(Anderson & Lozhkin, 2015; Einsele et al., 2001). Changes in sedimentation rates due to temporal variability in available moisture may also regulate the preservation of organic carbon within lacustrine sediments by affecting the time available for oxygen exposure and hence microbial degradation (Einsele et al., 2001). Higher Holocene sedimentation rates at Lake

Rauchuagytygn resulting from increased precipitation, active layer thickness and aeolian input may thus have further contributed to enhanced Holocene carbon accumulation. Lake area likely also plays a role in modulating differences in accumulation between lake sites and regions (Kastowski et al., 2011). Generally lakes of greater surface area possess lower rates of carbon accumulation due to reduced carbon loading (Ferland et al., 2012) (Fig. 9a). As geomorphic systems are hierarchical and operate at multiple spatio-temporal scales according to the concept of geomorphic connectivity, the diverse linkages and interrelationships between different catchment components and processes likely plays a large and complex role in regulating sediment and carbon dynamics at Lake Rauchuagytgyn (Singh et al., 2021). Anthropogenic factors can also impact upon organic matter dynamics by changing the land use dynamics within lake catchments (Biskaborn et al., 2021). However, the current pristine nature of the Lake Rauchuagytgyn catchment and the low occurrence of human activity, limits the anthropogenic influence when compared with lake catchments from more populous, lower latitude regions (Kastowski et al., 2011). Nonetheless, the future impact of exploration and mining operations within the catchment and of climate change within the permafrost landscape could lead to future changes in sediment and carbon dynamics that are yet to be seen (Tranvik et al., 2009).

Differences in accumulation calculation and hence rates can also arise due to diverging methodological approaches that can lead to significant bias. The necessary usage of empirical equations to estimate sediment volumes (Campbell et al., 2000) owed to missing data or the simplification of sediment volumes to a "box" form by combining deposit thickness with area (Jongejans et al., 2018; Windirsch et al., 2020) can lead to the introduction of very large uncertainty regarding pool calculations. Volume uncertainty within our study has been minimised through the usage of hydroacoustic methods. Despite this, hydroacoustic methods can be limited to a lesser degree by acoustic blanking and hence data absence in some areas and difficulty in tracing sometimes poorly resolved reflectors. Further methodological uncertainty can arise through oversimplified estimation of dry bulk density (DBD) from empirical equations of DBD and carbon content where discrete, volumetric measurements do not exist (Avnimelech et al., 2001; Kastowski et al., 2011) as well as varied approaches used for the measurement of sample carbon contents (Elemental analyser vs LOI) (Munroe and Brencher, 2019). Limitations associated with radiocarbon dating of Arctic glacial lakes due to the absence of appreciable amounts of datable organic material, particularly during glacial phases as well as the reworking of old organic carbon present within catchment sediments that can be brought to the lake basin through permafrost and glacial processes during warm and cold phases respectively, can additionally lead to uncertainty with regards to sediment ages and hence reconstructed accumulation rates (Abbott & Stafford, 1996; Björck & Wohlfarth 2002; Oswald et al., 2005). Despite this, the calculated OCARs and pools for Lake Rauchuagytgyn are largely agreeable with multiple studies from northern regions and reinforce the reliability, applicability and novelty of the presented results.

6. Conclusions:

This study aimed to improve the understanding of accumulation rates and pools within a palaeoenvironmental context of a Chukotkan Arctic glacial lake. The major outcomes are as follows:

- Sediment and carbon accumulation at Lake Rauchuagytgyn since MIS2 can be partitioned into three principal regimes (early MIS2, Mid MIS2-early MIS1 and Holocene accumulation) distinguished clearly from multiple environmental proxy records and calculated accumulation rates and pools.

- Early MIS2 accumulation (ca. 29–23.4 cal. ka BP) was controlled by cold glacial-periglacial conditions, quasi-permanent lake surface ice cover, the presence of a catchment glacier, and low sediment availability that led generally to low mass (MARs) and organic carbon accumulation rates (OCARs) and glacially-derived minerogenic sediment deposition.

- Mid MIS2-early MIS1 accumulation (ca. 23.4–11.69 cal. ka BP) likely reflects the increasing influence of paraglacial processes, longer surface ice-free summers, a thickening catchment active layer and increasing moisture availability. Carbon accumulation increased throughout and accompanied progressive climate amelioration.

- Holocene (ca. 11.69 cal. ka BP – present) accumulation reflects a warmer and wetter climate with enhanced runoff within a deglaciated catchment that led to alluvial fan activation and enhanced catchment fluvial dynamics. Ice-free summers likely led to increased wind-driven processes leading to more oxygenated lacustrine conditions during the mid-late Holocene and sediment redistribution. Higher Holocene OCARs reflect the prevailing climatic conditions and possibly the increased preservation under enhanced sedimentation rates.

- Estimated organic carbon pools reflect the presented accumulation regimes and demonstrates the larger carbon pool preserved within Holocene sediments (0.15 ± 0.005 Mt) when compared with Pleistocene sediments (0.1 ± 0.007 Mt). The carbon pool is however significantly small in comparison to the total sediment pool (25.7 ± 1.71 Mt).

- Carbon pools estimated for Finnish lake and Yakutian yedoma sediments show the greatest similarity to pools calculated for Lake Rauchuagytgyn sediments. Baldwin Peninsula (Alaska) permafrost landscapes and Alberta glacial lakes (Canada) represent larger organic carbon pools.

- Lake Rauchuagytgyn OCARs resemble estimations for Lake Baikal, Finnish and Canadian boreal and proglacial and bedrock-catchment Greenlandic lakes . Estimated rates are however significantly lower than the global lake mean as well as Cherskii-Kolyma thermokarst lakes in Far East Russia.

- The main drivers of OCAR and carbon pools on a temporal scale are likely related to palaeoclimate variations that control catchment and within-lake processes. Spatial differences with other lake systems are related to the high-latitude, mountainous setting of Lake Rauchuagytgyn.

Data availability

Data used in this study is accessible from the PANGAEA data repository https://doi.pangaea.de/10.1594/PANGAEA.929719.

Supplement

See separate supplement file

Author contributions

BB and UH designed the study and together with LP organised field–work. SAV obtained hydroacoustic profiling data and was responsible for opening, splicing and subsampling the core as well as all biogeochemical and sedimentological analyses. He also wrote the first version of the manuscript. GP was responsible for the age-depth model and sedimentation rates. NN provided magnetic susceptibility data. BB supervised the works of SAV. BD assisted in the interpretation of hydroacoustic data. All co-authors contributed to interpretation of the results and commented on the text.

Competing interests

The authors declare that they have no conflict of interest.

Acknowledgments

10. References

835 Abbott, M. B. & Stafford Jr, T. W.: Radiocarbon Geochemistry of Modern and Ancient Arctic Lake Systems, Baffin Island, Canada, Quat. Res., 45, 300–311, https://doi.org/10.1006/qres.1996.0031, 1996.

Adrian, R., O'Reilly, C. M., Zagarese, H., Baines, S. B., Hessen, D. O., Keller, W., Livingstone, D. M.,
840 Sommaruga, R., Straile, D., Van Donk, E., Weyhenmeyer, G. A., & Winder, M.: Lakes as sentinels of climate change, Limnol. Oceanogr., 54, 2283–2297, https://doi.org/10.4319/lo.2009.54.6_part_2.2283, 2009.

Alin, S. R. & Johnson, T. C.: Carbon cycling in large lakes of the world: A synthesis of production,
845 Global Biogeochem. Cycles, 21, GB3002, https://doi:10.1029/2006GB002881, 2007.

Anthony, K., Zimov, S., Grosse, G. et al.: A shift of thermokarst lakes from carbon sources to sinks during the Holocene epoch, Nature, 511, 452–456. https://doi.org/10.1038/nature13560, 2014.

850 Andersen, D. W., Wharton, R. A. Jr., Squyres S. W.: Terrigenous clastic sedimentation in Antarctic Dry Valley Lakes, Antarct Res Ser., 59, 71–81, 1993.

Anderson, N.J., D'Andrea, W. and Fritz, S.C.: Holocene carbon burial by lakes in SW Greenland, Glob. Change Biol., 15, 2590–2598. https://doi:10.1111/j.1365-2486.2009.01942.x, 2009.

855

Anderson, P.M., Lozhkin, A.V.: Late quaternary vegetation of Chukotka (northeast Russia) implications for glacial and Holocene environments of Beringia, Quat. Sci. Rev., 107, 112-128. https://doi.org/10.1016/j.quascirev.2014.10.016, 2015.

860 Andreev, A.A., Raschke, E., Biskaborn, B.K., Vyse, S.V., Courtin, J., Böhmer, T., Stoof-Leichsenring, K., Kruse, S., Pestryakova, L.A., Herzschuh, U.H.: Late Pleistocene to Holocene vegetation and climate changes in northwestern Chukotka (Far East Russia) deduced from lakes Ilirney and Rauchuagytgyn pollen records, Boreas, 2021.

865

Arnaud, F., Révillon, S., Debret, M., Revel, M., Chapron, E., Jacob, J., Giguet-Covex, C., Poulenard, J., Magny, M.: Lake Bourget regional erosion patterns reconstruction reveals Holocene NW European Alps soil evolution and paleohydrology, Quat. Sci. Rev., 51, 81–92. https://doi.org/10.1016/j.quascirev.2012.07.025, 2012.

870

Asikainen, C.A., Francus, P. & Brigham-Grette, J.: Sedimentology, clay mineralogy and grain-size as indicators of 65 ka of climate change from El'gygytgyn Crater Lake, Northeastern Siberia. J Paleolimnol., 37, 105–122. https://doi.org/10.1007/s10933-006-9026-5, 2007.

875 Avnimelech, Y., Ritvo, G., Meijer, L., Kochba, M.: Water content, organic carbon and dry bulk density in flooded sediments, Aquac. Eng., 25, 25–33, 2001.

Bakke, J., Lie, øyvind, Nesje, A., Dahl, S.O., Paasche, ø.: Utilizing physical sediment variability in glacier-fed lakes for continuous glacier reconstructions during the Holocene, northern Folgefonna,
880 western Norway, Holocene, 15, 161–176. https://doi.org/10.1191/0959683605hl797rp, 2005.

Ballantyne, C. K.: Paraglacial geomorphology, Quat. Sci. Rev., 21, 18–19, 1935–2017, https://doi.org/10.1016/S0277-3791(02)00005-7, 2002.

885   Battin, T. J., S. Luyssaert, L. A. Kaplan, A. K. Aufdenkempe, A. Richter, and L. J. Tranvik, L. J.: The boundless carbon cycle, Nat. Geosci., 2, 598–600, https://doi:10.1038/ngeo618, 2009.

       Battarbee, R.W., Jones, V.J., Flower, R.J., Cameron, N.G., Bennion, H., Carvalho, L., Juggins, S.: Diatoms, In: Tracking Environmental Change Using Lake Sediments, edited by Birks, H.J.B., Last,
890   W.M., Smol, J.P., Kluwer Academic Publishers, Dordrecht, Netherlands, 155–202, 2001.

       Baron, J., McKnight, D. & Denning, A.S.: Sources of dissolved and particulate organic material in Loch Vale Watershed, Rocky Mountain National Park, Colorado, USA, Biogeochemistry, 15, 89–110, https://doi.org/10.1007/BF00003219, 1991.
895
       Baster I., Girardclos S., Pugin A., Wildi W.: High-resolution seismic stratigraphy of an Holocene lacustrine delta in western Lake Geneva (Switzerland), In: Lake Systems from the Ice Age to Industrial Time, edited by Ariztegui, D., Wildi, W., Eclogae Geologicae Helvetiae / Swiss Journal of Geosciences, vol 1 , Birkhäuser, Basel. https://doi.org/10.1007/978-3-0348-7992-7_3, 2003.

900
       Baumer, M. M., Wagner, B., Meyer, H., Leicher, N., Lenz, M., Fedorov, G., Pestryakova, L. A. & Melles, M.: Climatic and environmental changes in the Yana Highlands of north-eastern Siberia over the last c. 57 000 years, derived from a sediment core from Lake Emanda, Boreas, 50, 114–133. https://doi.org/10.1111/bor.12476, 2020.

905
       Berger, A. & Loutre, M.F.: Insolation values for the climate of the last 10 million years, Quat. Sci. Rev., 10, 297–317, 1991.

       Birks, H.H., Birks, H.J.B.: Multi-proxy studies in palaeolimnology, Veget Hist Archaeobot, 15, 235–251
910   https://doi.org/10.1007/s00334-006-0066-6, 2006.

       Biskaborn, B.K., Herzschuh, U., Bolshiyanov, D., Savelieva, L., Diekmann, B.: Environmental variability in northeastern Siberia during the last ~13,300 yr inferred from lake diatoms and sediment-geochemical parameters, Palaeogeogr. Palaeoclimatol. Palaeoecol., 329–330, 22–36,
915   https://doi.org/10.1016/j.palaeo.2012.02.003, 2012.

       Biskaborn, B.K., Herzschuh, U., Bolshiyanov, D.Y., Schwamborn, G., Diekmann, B.: Thermokarst processes and depositional events in a tundra lake, northeastern Siberia. Permafr. Periglac. Process., 24, 160–174. https://doi.org/10.1002/ppp.1769, 2013.
920

       Biskaborn, B.K, Subetto, D., Savelieva, L,. Vakhrameeva, P., Hansche, A., Herzschuh, U., Klemm, J., Heinecke, L., Pestryakova, L., Meyer, H., Kuhn, G., Diekmann, B.: Late Quaternary vegetation and lake system dynamics in north-eastern Siberia: Implications for seasonal climate variability, Quat. Sci.
925   Rev., 147, 406–421, https://doi.org/10.1016/j.quascirev.2015.08.014, 2016.

       Biskaborn, B.K., Nazarova, L., Pestryakova, L.A., Syrykh, L., Funck, K., Meyer, H., Chapligin, B., Vyse, S., Gorodnichev, R., Zakharov, E., Wang, R., Schwamborn, G., Bailey, H.L., Diekmann, B.: Spatial distribution of environmental indicators in surface sediments of Lake Bolshoe Toko, Yakutia, Russia.
930   Biogeosciences 16, 4023-4049, https://doi.org/10.5194/bg-16-4023-2019, 2019.

       Biskaborn, B.K., Narancic, B., Stoof-Leichsenring, K.R., Pestryakova, L.A., Appleby, P.G., Piliposian, G.T., Diekmann, B.: Effects of climate change and industrialization on Lake Bolshoe Toko, eastern Siberia. J. Paleolimnol., 65, 335–352, https://doi.org/10.1007/s10933-021-00175-z, 2021.

935
       Björck, S. & Wohlfarth, B.: 14C chronostratigraphic techniques in paleolimnology, In: Tracking environmental change using lake sediments. Basin Analysis, Coring, and Chronological Techniques, edited by Last, W. M. & Smol, J. P., Springer, Dordrecht, Netherlands, 205–245, 2002.

940   Blott, S.J. & Pye, K.: GRADISTAT: A grain size distribution and statistics package for the analysis of unconsolidated sediments, Earth Surf. Proc. Land., 26, 1237–1248. https://doi.org/10.1002/esp.261, 2001.

Bouchard, F., Francus, P., Pienitz, R., Laurion, I.: Sedimentology and geochemistry of thermokarst
945   ponds in discontinuous permafrost, subarctic Quebec, Canada. J. Geophys. Res., 116, G00M04, https://doi:10.1029/2011JG001675, 2011.

Bouchard, F., MacDonald, L.A., Turner, K.W., Thienpont, J.R., Medeiros, A.S., Biskaborn, B.K., Korosi, J., Hall, R.I., Pienitz, R., and Wolfe, B.B.: Paleolimnology of thermokarst lakes: a window into
950   permafrost landscape evolution, Arctic Science, 3(2), 91-117, https://doi.org/10.1139/as-2016-0022, 2016.

Brigham-Grette, J., Gualtieri, L.M., Glushkova, O.Y., Hamilton, T.D., Mostoller, D., Kotov, A.: Chlorine-36 and 14C chronology support a limited last glacial maximum across central Chukotka, northeastern
955   Siberia, and no Beringian ice sheet, Quat. Res., *59*, 386–398. https://doi.org/10.1016/S0033-5894(03)00058-9, 2003.

Brosius, L.S., Walter Anthony, K.M., Treat, C.C., Lenz, J., Jones, M.C., Bret-Harte, M.S., Grosse, G.: Spatiotemporal patterns of northern lake formation since the Last Glacial Maximum, Quat. Sci. Rev.,
960   253, https://doi.org/10.1016/j.quascirev.2020.106773, 2021.

Bunbury, J., Finkelstein, S. A., Bollman, J.: Holocene hydro-climatic change and effects on carbon accumulation inferred from a peat bog in the Attawapiskat River watershed, Hudson Bay Lowlands, Canada. Quat. Res., 78, 275–284, 2012.

965

Bünseler, L.: Interaction of active layer carbon and nitrogen content with vegetation types on a tundra to taiga transect in eastern Siberia, MSc thesis, Potsdam University, Potsdam, Germany, 2019.

Campbell, I.D., Campbell, C., Vitt, D.H., Kelker, D., Laird, L.D., Trew, D., Kotak, B., LeClair, D., Bayley,
970   S.: A first estimate of organic carbon storage in Holocene lake sediments in Alberta, Canada, J. Paleolimnol., 24(4), 395–400, https://doi:10.1023/A:1008103605817, 2000.

Canty, A., Ripley, B. D.: boot: Bootstrap R (S-Plus) Functions, R package version 1.3–26, 2020.

975   Cole, J. J., Prairie, Y. T., Caraco, N. F., McDowell, W. H., Tranvik, L. J., Striegl, R. G., Duarte, C. M., Kortelainen, P., Downing, J. A., Middelburg J. J. and Melack, J.: Plumbing the global carbon cycle: Integrating inland waters into the terrestrial carbon pool, Ecosystems, 10(1), 172–185, https://doi:10.1007/s10021-006-9013-8, 2007.

980   Cremer, H., Wagner, B.: The diatom flora in the ultra-oligotrophic Lake El'gygytgyn, Chukotka. Polar Biol., 26, 105–114. https://doi.org/10.1007/s00300-002-0445-0, 2003.

Croudace, I.W., Rothwell, R.G. (Eds.): Micro-XRF Studies of Sediment Cores: Applications of a non-destructive tool for the environmental sciences, Springer, Netherlands, https://doi.org/10.1007/978-94-
985   017-9849-5, 2015.

Cuven, S., Francus, P. & Lamoureux, S.F.: Estimation of grain size variability with micro X-ray fluorescence in laminated lacustrine sediments, Cape Bounty, Canadian High Arctic. J Paleolimnol., 44, 803–817. https://doi.org/10.1007/s10933-010-9453-1, 2010.

990

D'Arcy, P., and Carignan, R.: Influence of catchment topography on water chemistry in southeastern Québec shield lakes, Can. J. Fish. Aquat. Sci., 54(10), 2215–2227, https://doi:10.1139/f97-129, 1997.

995   Davison, A.C., Hinkley, D.V. (Eds.): Bootstrap Methods and Their Applications, Cambridge University Press, Cambridge, http://statwww.epfl.ch/davison/BMA/, 1997.

Dean, W. E., and Gorham, E.: Magnitude and significance of carbon burial in lakes, reservoirs, and peatlands, Geology, 26(6), 535–538, https://doi:10.1130/00917613(1998)026<0535:MASOCB>2.3.CO;2, 1998.

1000

Dedkov, A.: The relationship between sediment yield and drainage basin area. Sediment Transfer through the Fluvial System (Proceedings of a symposium held in Moscow. August 2004), IAHS Publ. 288, 2004.

1005   Diekmann, B., Pestryakova, L., Nazarova, L., Subetto, D., Tarasov, P., Stauch, G., Thiemann, A., Lehmkuhl, F., Biskaborn, B., Kuhn, G., Henning, D., Müller, S.: Late Quaternary lake dynamics in the Verkhoyansk Mountains of eastern Siberia: Implications for climate and glaciation history, Polarforschung, 86, 97–110. https://doi.org/10.2312/polarforschung.86.2.97, 2016.

1010   Dietze, E., Maussion, F., Ahlborn, M., Diekmann, B., Hartmann, K., Henkel, K., Kasper, T., Lockot, G., Opitz, S., Haberzettl, T.: Sediment transport processes across the Tibetan Plateau inferred from robust grain-size end members in lake sediments, Clim. Past, 10, 91–106, https://doi.org/10.5194/cp-10-91-2014, 2014.

1015   Doran, P.T.: Sedimentology of Colour Lake, a Nonglacial High Arctic Lake, Axel Heiberg Island, N.W.T., Canada, Arctic and Alpine Research, 25:4, 353–367, https://doi:10.1080/00040851.1993.12003021, 1993.

1020   Einola, E., Rantakari, M., Kankaala, P., Kortelainen, P., Ojala, A., Pajunen, H., Mäkelä, S., and Arvola, L.: Carbon pools and fluxes in a chain of five boreal lakes: A dry and wet year comparison, J. Geophys. Res., 116, G03009, https://doi:10.1029/2010JG001636, 2011.

Einsele, G., Yan, J.P., and Hinderer, M.: Atmospheric carbon burial in modern lake basins and its significance for the global carbon budget, Glob. Planet. Change, 30(3–4), 167–195,
1025   https://doi:10.1016/S0921-8181(01)00105-9, 2001.

Elias, S. A. & Brigham-Grette, J.: Glaciations: Late Pleistocene glacial events in Beringia, In: Encyclopedia of Quaternary Science, edited by: Elias, S. A., Elsevier, Amsterdam, 191–201, 2013.

1030   Ferland, M.E., del Giorgio, P. A., Teodoru, C. R., and Prairie, Y. T.: Long-term C accumulation and total C stocks in boreal lakes in northern Québec, Global Biogeochem. Cycles, 26, GB0E04, doi:10.1029/2011GB004241, 2012.

Ferland, M.E., Prairie, Y. T., Teodoru, C., and del Giorgio, P. A.: Linking organic carbon sedimentation,
1035   burial efficiency, and long-term accumulation in boreal lakes, J. Geophys. Res. Biogeosci., 119, 836–847, doi:10.1002/2013JG002345, 2014.

Finkenbinder, M.S., Abbott, M.B., Edwards, M.E., Langdon, C.T., Steinman, B.A., Finney, B.P.: A 31,000 year record of paleoenvironmental and lake-level change from Harding Lake, Alaska, USA,
1040   Quat. Sci. Rev., 87, 98–113, https://doi.org/10.1016/j.quascirev.2014.01.005, 2014.

Finkenbinder, M.S., Abbott, M.B., Finney, B.P., Stoner, J.S., Dorfman, J.M.: A multi-proxy reconstruction of environmental change spanning the last 37,000 years from Burial Lake, Arctic Alaska, Quat. Sci. Rev, 126, 227–241, https://doi.org/10.1016/j.quascirev.2015.08.031, 2015.

1045

Folk, R.L. and Ward, W.C.: Brazos River bar [Texas]; a study in the significance of grain size parameters, J. Sediment. Res, 27 (1): 3–26, doi: https://doi.org/10.1306/74D70646-2B21-11D7-8648000102C1865D, 1957.

1050 Francke, A., Wennrich, V., Sauerbrey, M., Juschus, O., Melles, M. & Brigham-Grette, J.: Multivariate statistic and time series analyses of grain-size data in quaternary sediments of Lake El'gygytgyn, NE Russia, Clim. Past, 9, 2459–2470, https://doi.org/10.5194/cp-9-2459-2013, 2013.

Friedman, G.M. and Sanders, J.E. (Eds): Principles of Sedimentology, Wiley, New York, 1978.

1055

Frihmat, Y., Hebbeln, D., Jaaidi, El., Mhammdi, N.: Reconstruction of productivity signal and deep-water conditions in Moroccan Atlantic margin (~35°N) from the last glacial to the Holocene, Springerplus 4, 69, https://doi.org/10.1186/s40064-015-0853-6, 2015.

1060 Fritz, M., Unkel, I., Lenz, J., Gajewski, K., Frenzel, P., Paquette, N., Lantuit, H., Körte, L., Wetterich, S.: Regional environmental change versus local signal preservation in Holocene thermokarst lake sediments: A case study from Herschel Island, Yukon (Canada), J Paleolimnol., 60, 77–96 https://doi.org/10.1007/s10933-018-0025-0, 2018.

1065 Gentz, T. , Bonk, E. , Hefter, J. , Grotheer, H. , Meyer, V. and Mollenhauer, G.: Establishment of routine sample preparation protocols at the newly installed MICADAS 14C dating facility at AWI , AMS 14 Conference, Ottawa, 14 August 2017 - 18 August 2017.

Glushkova, O. Y.: Chapter 63 - Late Pleistocene Glaciations in North-East Asia, In: Developments in
1070 Quaternary Sciences, edited by: Jürgen Ehlers, Philip L. Gibbard, Philip D. Hughes, Elsevier, Amsterdam, 865–875 https://doi.org/10.1016/B978-0-444-53447-7.00063-5, 2011.

Glückler, R., Herzschuh, U., Kruse, S., Andreev, A., Vyse, S. A., Winkler, B., Biskaborn, B. K., Pestryakova, L., Dietze, E.: Wildfire history of the boreal forest of southwestern Yakutia (Siberia)
1075 over the last two millennia documented by a lake-sedimentary charcoal record, Biogeosciences Discuss. https://doi.org/10.5194/bg-2020-415, 2020.

Gromig, R., Wagner, B., Wennrich, V., Fedorov, G., Savelieva, L., Lebas, E., Krastel, S., Brill, D., Andreev, A., Subetto, D. & Melles, M.: Deglaciation history of Lake Ladoga (northwestern Russia)
1080 based on varved sediments, Boreas, 48, 330–348. https://doi.org/10.1111/bor.12379, 2019.

Gurnell, A., Hannah, D., Lawler, D: Suspended sediment yield from glacier basins, Erosion and Sediment Yield: Global and Regional Perspectives (Proceedings of the Exeter Symposium, July 1996).

1085 Haflidason, H., Zweidorff, J. L., Baumer, M., Gyllencreutz, R., Svendsen, J. I., Gladysh, V. & Logvina, E.: The Lastglacial and Holocene seismostratigraphy and sediment distribution of Lake Bolshoye Shchuchye, Polar Ural Mountains, Arctic Russia, Boreas, 48, 452–469, https://doi.org/10.1111/bor.12387, 2019.

1090 Hamilton, T., Ashley, G.: Epiguruk: a late Quaternary environmental record from northwestern Alaska, GSA Bull., 105, 583–602. https://doi.org/10.1130/0016-7606(1993)105<0583:ealger>2.3.co;2, 1993.

Heinecke, L., Mischke, S., Adler, K. et al.: Climatic and limnological changes at Lake Karakul (Tajikistan) during the last ~29 cal ka, J. Paleolimnol., 58, 317–334, https://doi.org/10.1007/s10933-017-9980-0, 2017.

Hinderer, M., Einsele, G.: The world's large lake basins as denudation-accumulation systems and implications for their lifetimes, J Paleolimnol., 26, 355–372, https://doi.org/10.1023/A:1012651232541, 2001.

Horiuchi K., Kobayashi K., Oda T., Nakamura T. and Fujimura C.: Climate-induced fluctuations of 10Be concentration in Lake Baikal sediments. Nucl. Instrum. Meth. Phys. Res., 562–567, 2000.

Huang, S., Herzschuh, U., Pestryakova, L. A., Zimmermann, H. H., Davydova, P., Biskaborn, B. K., Shevtsova, I., & Stoof-Leichsenring, K. R.: Genetic and morphologic determination of diatom community composition in surface sediments from glacial and thermokarst lakes in the Siberian Arctic. J Paleolimnol., 64, 225–242. https://doi.org/10.1007/s10933-020-00133-1, 2020.

Jenrich, M., Angelopoulos, M., Grosse, G., Overduin, P.P., Schirrmeister, L., Nitze, I., Biskaborn, B.K., Liebner, S., Grigoriev, M., Murray, A., Strauss, J.: Thermokarst Lagoons on Bykovsky Peninsula: A Core-Based Assessment of Depositional Characteristics and Estimate of Carbon Pools, Frontiers in Earth Science, accepted.

Jongejans, L., Strauss, J., Lenz, J., Peterse, F., Mangelsdorf, K., Fuchs, M., Grosse, G.: Organic matter characteristics in Yedoma and thermokarst deposits on Baldwin Peninsula, west Alaska. Biogeosciences, 15, 6033–6048, https://doi.org/10.5194/bg-15-6033-2018, 2018.

Jongejans, L., & Strauss, J.: Bootstrapping approach for permafrost organic carbon pool estimation, Zenodo, http://doi.org/10.5281/zenodo.3734247, 2020.

Karlen, W and Matthews, J.A.: Reconstructing Holocene Glacier Variations from Glacial Lake Sediments: Studies from Nordvestlandet and Jostedalsbreen-Jotunheimen, Southern Norway, Geografiska Annaler. Series A, Physical Geography, 74, 327–348, 1992.

Kastowski, M., Hinderer, M. & Vecsei, A.: Long-term carbon burial in European lakes: Analysis and estimate, Glob. Biogeochem. Cycles, 25, GB3019, http://doi:10.1029/2010GB003874, 2011.

Kilian, R., Baeza, O., Breuer, S., Ríos, F., Arz, H., Lamy, F., Wirtz, J., Baque, D., Korf, P., Kremer, K., Ríos, C., Mutschke, E., Simon, M., De Pol-Holz, R., Arevalo, M., Wörner, G., Schneider, C & Casassa, G: Late Glacial and Holocene Paleogeographical and Paleoecological Evolution of the Seno Skyring and Otway Fjord Systems in the Magellan Region, Anales Instituto Patagonia (Chile), 41, 5–26, http://dx.doi.org/10.4067/S0718-686X2013000200001, 2013.

Kokorowski, H.D., Anderson, P.M., Mock, C.J., Lozhkin, A.V.: A re-evaluation and spatial analysis of evidence for a Younger Dryas climatic reversal in Beringia. Quat. Sci. Rev., 27, 1710–1722, https://doi.org/10.1016/j.quascirev.2008.06.010, 2008b.

Kokorowski, H.D., Anderson, P.M., Sletten, R.S., Lozhkin, A.V., & Brown T.A.: Late Glacial and Early Holocene Climatic Changes Based on a Multiproxy Lacustrine Sediment Record from Northeast Siberia, Arct. Antarct. Alp. Res., 40:3, 497–505, https://doi.org/10.1657/1523-0430(07-036), 2008a.

Kortelainen, P., Pajunen, H., Rantakari, M and Saarnisto M.: A large carbon pool and small sink in boreal Holocene lake sediments, Global Change Biol., 10(10), 1648–1653, https://doi:10.1111/j.1365-2486.2004.00848.x, 2004.

Křibek, B., Knésl, I., Rojík, P., Sýkorová, I., Martínek, K.: Geochemical history of a Lower Miocene lake, the Cypris Formation, Sokolov Basin, Czech Republic, J Paleolimnol., 58, 169–190, https://doi.org/10.1007/s10933-017-9970-2, 2017.

1150   Lebas, E., Krastel, S., Wagner, B., Gromig, R., Fedorov, G., Baumer, M., Kostromina, N., Haflidason, H.: Seismic stratigraphical record of Lake Levinson-Lessing, Tayma Peninsula: evidence for ice-sheet dynamics and lake-level fluctuations since the Early Weichselian. Boreas, 48, 470–487, https://doi.org/10.1111/bor.12381, 2019.

1155   Lebas, E., Gromig, R., Krastel, S., Wagner, B., Fedorov, G., Görtz, C., Averes, T., Subetto, D., Naumenko, M., Melles, M.: Pre-glacial and post-glacial history of the Scandinavian Ice Sheet in NW Russia – Evidence from Lake Ladoga, Quat. Sci. Rev., 251, https://doi.org/10.1016/j.quascirev.2020.106637, 2021.

1160   Leemann A, Niessen F.: Holocene glacial activity and climatic variations in the Swiss Alps: reconstructing a continuous record from proglacial lake sediments, The Holocene, 4(3): 259–268, doi:10.1177/095968369400400305, 1994b.

        Lehman, J. T.: Reconstructing the rate of accumulation of lake sediment: Their effect of sediment
1165   focusing, Quat. Res., 5(4), 541–550, https://doi:10.1016/0033-5894(75)90015-0, 1975.

        Lenz, M., Savelieva, L., Frolova, L., Cherezova, A., Moros, M., Baumer, M. M., Gromig, R., Kostromina, N., Nigmatullin, N., Kolka, V., Wagner, B., Fedorov, G. & Melles, M.: Lateglacial and Holocene environmental history of the central Kola region, northwestern Russia revealed by a sediment
1170   succession from Lake Imandra, Boreas, 50, 76–100, https://doi.org/10.1111/bor.12465. ISSN 0300-9483, 2020.

        Lougheed, B.C., Obrochta, S.P.: A Rapid, Deterministic Age-Depth Modeling Routine for Geological Sequences With Inherent Depth Uncertainty. Paleoceanogr. Paleoclimatol., 34, 122–133,
1175   https://doi.org/10.1029/2018PA003457, 2019.

        Lozhkin, A.V., Anderson, P.M.: Late quaternary lake records from the Anadyr lowland, central Chukotka (Russia). Quat. Sci. Rev., 68, 1–16. https://doi.org/10.1016/j.quascirev.2013.02.007, 2013.

1180   Lozhkin, A.V., Brown, T.A., Anderson, P.M., Glushkova, O.Y., Melekestsev, I. V.: The importance of radiocarbon dates and tephra for developing chronologies of Holocene environmental changes from lake sediments, North Far East, Russ. J. Pac. Geol., 10, 249–262. https://doi.org/10.1134/S1819714016040047, 2016.

1185   Lozhkin, A.V., Anderson, P.M., Minyuk, P., Korzun, J., Brown, T., Pakhomov, A., Tsygankova, V., Burnatny, S., Naumov, A.: Implications for conifer glacial refugia and postglacial climatic variation in western Beringia from lake sediments of the Upper Indigirka basin, Boreas, 47, 938–953. https://doi.org/10.1111/bor.12316, 2018.

1190   Lunkka, J.P., Saarnisto, M., Gey, V., Demidov, I., Kiselova, V.: Extent and age of the Last Glacial Maximum in the southeastern sector of the Scandinavian Ice Sheet, Glob. Planet. Change, 31, 407–425, https://doi.org/10.1016/S0921-8181(01)00132-1, 2001.

1195   Martin, P., L. Granina, K.Martens, and B. Goddeeris.: Oxygen concentration profiles in sediments of two ancientlakes: Lake Baikal (Siberia, Russia) and Lake Malawi (EastAfrica), Hydrobiologia, 367, 163–174, https://doi.org/10.1023/A:1003280101128, 1998.

Marshall, M.H., Lamb, H.F., Huws, D., Davies, S.J., Bates, R., Bloemendal, J., Boyle, J., Leng, M.J., Umer, M., Bryant, C.: Late Pleistocene and Holocene drought events at Lake Tana, the source of the Blue Nile. Glob. Planet. Change, 78, 147–161, https://doi.org/10.1016/j.gloplacha.2011.06.004, 2011.

Mattsson, T., P. Kortelainen, and Räike, A.: Export of DOM from boreal catchments: Impacts of land use cover and climate, Biogeochemistry, 76, 373–394, https://doi:10.1007/s10533-005-6897-x, 2005.

McLaren, P., Bowles, D.: The effects of sediment transport on grain-size distributions, Int. J. Sediment Res., 55 (4), 457–470, https://doi.org/10.1306/212F86FC-2B24-11D7-8648000102C1865D, 1985.

Melles, M., Brigham-Grette, J., Glushkova, O.Y., Minyuk, P.S., Nowaczyk, N.R., Hubberten, H.W.: Sedimentary geochemistry of core PG1351 from Lake El'gygytgyn-a sensitive record of climate variability in the East Siberian Arctic during the past three glacial-interglacial cycles. J. Paleolimnol., 37, 89–104, https://doi.org/10.1007/s10933-006-9025-6, 2007.

Melles, M., Brigham-Grette, J., Minyuk, P.S., Nowaczyk, N.R., Wennrich, V., DeConto, R.M., Anderson, P.M., Andreev, A.A., Coletti, A., Cook, T.L., Haltia-Hovi, E., Kukkonen, M., Lozhkin, A. V., Rosén, P., Tarasov, P., Vogel, H., Wagner, B.: 2.8 Million years of arctic climate change from Lake El'gygytgyn, NE Russia, Science, 337, 315–320. https://doi.org/10.1126/science.1222135, 2012.

Mendonça, R., Müller, R.A., Clow, D., Verpoorter, C., Raymond, P., Tranvik, L.J & Sobek, S.: Organic carbon burial in global lakes and reservoirs, Nat. Commun., 8, 1694. https://doi.org/10.1038/s41467-017-01789-6

Meyer, H., Derevyagin, A. Y., Siegert, C. & Hubberten, H.W.: Paleoclimate studies on Bykovsky Peninsula, North Siberia-hydrogen and oxygen isotopes in ground ice. Polarforschung, 70, 37–51, 2002.

Meyers, P.A., Teranes, J.L.: Sediment organic matter, In: Tracking Environmental Change Using Lake Sediments, edited by Smol, J., Kluwer Academic Publishers, Dordrecht, 239–269. https://doi.org/10.1007/0-306-47670-3_9, 2005.

Meyers, Philip A.: Preservation of Elemental and Isotopic Source Identification of Sedimentary Organic Matter. Chem. Geol., 114 (3–4), 289–302. https://doi.org/10.1016/0009-2541(94)90059-0, 1994.

Menne, M.J., Durre, I., Korzeniewski, B., McNeal, S., Thomas, K., Yin, X, Anthony, S., Ray, R., Vose, R.S,. Gleason, B.E. & Houston, T.G.: Global Historical Climatology Network - Daily (GHCN-Daily), Version 3 NOAA National Climatic Data Center. https://doi:10.7289/V5D21VHZ, 2012.

Moernaut, J., Verschuren, D., Charlet, F., Kristen, I., Fagot, M., De Batist, M.: The seismic-stratigraphic record of lake-level fluctuations in Lake Challa: Hydrological stability and change in equatorial East Africa over the last 140ka, Earth Planet. Sci. Lett., 290, 214–223, https://doi.org/10.1016/j.epsl.2009.12.023, 2010.

Munroe, J., Brencher, Q.: Holocene Carbon Burial in Lakes of the Uinta Mountains, Utah, USA, Quaternary 2019, 2, 1–13, https://doi.org/10.3390/quat2010013, 2019.

Naeher, S., Gilli, A., North, R.P., Hamann, Y., Schubert, C.J.: Tracing bottom water oxygenation with sedimentary Mn/Fe ratios in Lake Zurich, Switzerland. Chem. Geol., 352, 125–133. https://doi.org/10.1016/j.chemgeo.2013.06.006, 2013.

1250   Nolan, M., Liston, G., Prokein, P., Brigham-Grette, J., Sharpton, V. L., and Huntzinger, R.: Analysis of lake ice dynamics and morphology on Lake El'gygytgyn, NE Siberia, using synthetic aperture radar (SAR) and Landsat, J. Geophys. Res., 107, 8162, https://doi.org/10.1029/2001JD000934, 2002.

Nolan, M., Brigham-Grette, J.: Basic hydrology, limnology, and meteorology of modern Lake
1255   El'gygytgyn, Siberia, J. Paleolimnol., 37, 17–35. https://doi.org/10.1007/s10933-006-9020-y, 2007.

Nowaczyk, N.R., Melles, M. & Minyuk, P.: A revised age model for core PG1351 from Lake El'gygytgyn, Chukotka, based on magnetic susceptibility variations tuned to northern hemisphere insolation variations, J. Paleolimnol., 37, 65–76 https://doi.org/10.1007/s10933-006-9023-8, 2007.
1260

Oswald, W.W., Anderson, P.M., Brown, T.A., Brubaker, L.B., Hu, F.S., Lozhkin, A.V., Tinner, W and Kaltenrieder, P.: Effects of sample mass and macrofossil type on radiocarbon dating of arctic and boreal lake sediments, The Holocene, 15, 758–767, 2005.

1265   Pajunen, H.: lake sediments: their carbon store and related accumulations rates, *spec. pap. geol. surv. finl.*, *29*, 39–69, 2000.

Pace, M. L., and Prairie Y. T.: Respiration in lakes, in Respiration in Aquatic Ecosystems, edited by P. A. del Giorgio and P. J. L. Williams, 103–121, Oxford Univ. Press, New York,
1270   https://doi:10.1093/acprof:oso/9780198527084.003.0007, 2005.

Pfalz, P., Diekmann, B., Freytag, J-C., Biskaborn, B.K.: Harmonizing heterogeneous multi-proxy data from lake systems, Comput Geosci,153, https://doi.org/10.1016/j.cageo.2021.104791, 2021.

1275   Píšková, A., Roman, M., Bulínová, M., et al.: Late-Holocene palaeoenvironmental changes at Lake Esmeralda (Vega Island, Antarctic Peninsula) based on a multi-proxy analysis of laminated lake sediment, The Holocene, 2019;29(7), 1155–1175, doi:10.1177/0959683619838033, 2019.

Procházka, V., Mizera, J., Kletetschka, G. et al.: Late Glacial sediments of the Stará Jímka paleolake
1280   and the first finding of Laacher See Tephra in the Czech Republic, Int J Earth Sci (Geol Rundsch) 108, 357–378, https://doi.org/10.1007/s00531-018-1658-y, 2019.

R Core Team.: R: A language and environment for statistical computing, R Foundation for Statistical Computing, Vienna, Austria. URL http://www.R-project.org/, 2013.
1285

Reimer, P.J., Austin, W.E.N., Bard, E., Bayliss, A., Blackwell, P.G., Bronk Ramsey, C., Butzin, M., Cheng, H., Edwards, R.L., Friedrich, M., Grootes, P.M., Guilderson, T.P., Hajdas, I., Heaton, T.J., Hogg, A.G., Hughen, K.A., Kromer, B., Manning, S.W., Muscheler, R., Palmer, J.G., Pearson, C., van der Plicht, J., Reimer, R.W., Richards, D.A., Scott, E.M., Southon, J.R., Turney, C.S.M., Wacker, L.,
1290   Adolphi, F., Büntgen, U., Capano, M., Fahrni, S.M., Fogtmann-Schulz, A., Friedrich, R., Köhler, P., Kudsk, S., Miyake, F., Olsen, J., Reinig, F., Sakamoto, M., Sookdeo, A., Talamo, S.: The IntCal20 Northern Hemisphere Radiocarbon Age Calibration Curve (0–55 Cal ka BP), Radiocarbon, 1–33, https://doi.org/10.1017/RDC.2020.41, 2020.

1295   Regnéll, C., Haflidason, H., Mangerud, J. & Svendsen, J. I.: Glacial and climate history of the last 24 000 years in the Polar Ural Mountains, Arctic Russia, inferred from partly varved lake sediments, Boreas, 48, 432–443, https://doi.org/10.1111/bor.12369. ISSN 0300-9483, 2019.

Schirrmeister, L., Grosse, G., Wetterich, S., Overduin, P.P, Strauss, J., Edward A. G. Schuur,
1300   Hubberten, H. W.: Fossil Organic Matter Characteristics in Permafrost Deposits of the Northeast Siberian Arctic, J. Geophys. Res., 116, G00M02. https://doi.org/10.1029/2011JG001647, 2011.

Sekellick, A., Banks, W., Myers, M.: Water Volume and Sediment Volume and Density in Lake Linganore between Boyers Mill Road Bridge and Bens Branch, Frederick County, Maryland. Scientific
1305   Investigations Report, *2013–5082* U.S. Department of the Interior, U.S. Geological Survey, 2013.

Sifeddine, A., Meyers, P., Cordeiro, R., Albuquerque, A., Bernardes, M., Turcq, B., Abra~o, J.: Delivery and deposition of organic matter in surface sediments of Lagoa do Caçó (Brazil), J. Paleolimnol., 45, 385–396, https://doi.org/10.1007/s10933-011-9506-0, 2011.

1310

Singh, M., Sinha, R., Tandon, S.K.: Geomorphic connectivity and its application for understanding landscape complexities: a focus on the hydro-geomorphic systems of India, Earth Surf. Process. Landf., 46, 110–130, 2020.

1315   Shevtsova, I., Heim, B., Kruse, S., Schröder, J., Troeva, E.I., Pestryakova, L.A., Zakharov E.S. & Herzschuh, U.: Strong shrub expansion in tundra-taiga, tree infilling in taiga and stable tundra in central Chukotka (north-eastern Siberia) between 2000 and 2017, Environ. Res. Lett., https://doi.org/10.1088/1748-9326/ab9059, 2020.

1320   Smith, D., Jol, H.: Radar structure of a Gilbert-type delta, Peyto Lake, Banff National Park, Canada, Sediment. Geol, 113, 195–209, https://doi.org/10.1016/S0037-0738(97)00061-4, 1997.

Smol, J.P., Birks, H.J.B., Last, W.M., (Eds.): Tracking environmental change using lake sediments, Kluwer academic publishers, New York, USA, 2002.

1325

Sobek, S., Tranvik, L., Prairie, Y., Kortelainen, P., Cole, Jonathan J.: Patterns and regulation of dissolved organic carbon: An analysis of 7,500 widely distributed lakes, Limnol. Oceanogr., 52, https://doi.org/10.4319/lo.2007.52.3.1208, 2007.

1330   Sobek, S., Durisch-Kaiser, E., Zurbrügg, R., Wongfun, N., Wessels, M., Pasche, N., Wehrli, B. Organic carbon burial efficiency in lake sediments controlled by oxygen exposure time and sediment source, Limnol. Oceanogr, 54, https://doi.org/10.4319/lo.2009.54.6.2243, 2009.

Sobek, S., Anderson, N. J., Bernasconi, S. M., Sontro T. D.: Low organic   carbon burial efficiency in
1335   arctic lake sediments, J. Geophys. Res. Biogeosci., 119, https://doi.org/10.1002/2014JG002612, 2014.

Stauch, G, Gualtieri, L.: Late Quaternary glaciations in northeastern Russia, J Quat Sci, 23, 545–558, https://doi.org/10.1002/jqs.1211, 2008.

1340

Stauch, G., Lehmkuhl, F.: Quaternary glaciations in the Verkhoyansk Mountains, Northeast Siberia, Quat. Res., 74, 145-155, https://doi.org/10.1016/j.yqres.2010.04.003, 2010.

Strauss, J., Schirrmeister, L., Grosse, G., Wetterich, S., Ulrich, M., Herzschuh, U., and Hubberten, H.-
1345   W.: The deep permafrost carbon pool of the Yedoma region in Siberia and Alaska, Geophys. Res. Lett., 40, 6165– 6170, doi:10.1002/2013GL058088, 2013.

Strunk, A., Olsen, J., Sanei, H., Rudra, A., Larsen, N.: Improving the reliability of bulk sediment radiocarbon dating, Quat. Sci. Rev., 242, 106442, https://doi.org/10.1016/j.quascirev.2020.106442,
1350   2020.

Stuiver, M., Reimer, P.J., Reimer, R.W.: CALIB 8.2, available at: http://calib.org, 2020.

Subetto, D.A., Nazarova, L.B., Pestryakova, L.A., Syrykh, L.S., Andronikov, A.V., Biskaborn, B.,
1355   Diekmann, B., Kuznetsov, D.D., Sapelko, T.V., Grekov, I.M.: Paleolimnological studies in Russian northern Eurasia: A review. Contemporary Problems of Ecology, 10, 327-335, 2017.

1360 Tranvik, Lars J., Downing, John A., Cotner, James B., Loiselle, Steven A., Striegl, Robert G., Ballatore, Thomas J., Dillon, Peter, Finlay, Kerri, Fortino, Kenneth, Knoll, Lesley B., Kortelainen, Pirkko L., Kutser, Tiit, Larsen, Soren., Laurion, Isabelle, Leech, Dina M., McCallister, S. Leigh, McKnight, Diane M., Melack, John M., Overholt, Erin, Porter, Jason A., Prairie, Yves, Renwick, William H., Roland, Fabio, Sherman, Bradford S., Schindler, David W., Sobek, Sebastian, Tremblay, Alain, Vanni, Michael J., Verschoor, Antonie M., von Wachenfeldt, Eddie, Weyhenmeyer, Gesa A.: Lakes and reservoirs as regulators of carbon cycling and climate, Limnol. Oceanogr. 54, 2298–2314,
1365 https://doi.org/10.4319/lo.2009.54.6_part_2.2298, 2009.

Tripathi, J., Rajamani, V.: Geochemistry of the loessic sediments on Delhi ridge, eastern Thar Desert, Rajasthan: implications for exogenic processes, Chem. Geol., 155, 265–278. https://doi.org/10.1016/S0009-2541(98)00168-5, 1999.
1370
Van der Bilt, W., Bakke, J., Vasskog, K., D´Andrea, W.J., Bradley, R.S., Ólafsdóttir, S.: Reconstruction of glacier variability from lake sediments reveals dynamic Holocene climate in Svalbard. Quat. Sci. Rev., 126, 15, 201–218. https://doi.org/10.1016/j.quascirev.2015.09.003, 2015.

1375 Vologina, E.G., Granin, N.G., Lomonosova, T.K., Vorobyeva, SS., Kulikova, N.A., Kalashnikova, I.A., Granina, L.Z.: Input of silt-sand material to the central part of southern lake Baikal by ice transportation, BAIK-SED-2, Gent University, Belgium, 17–18, 2003.

1380 Vyse, S.A., Herzschuh, U., Andreev, A.A., Pestryakova, L.A., Diekmann, B., Armitage, S.J., Biskaborn, B.K.: Geochemical and sedimentological responses of arctic glacial Lake Ilirney, chukotka (far east Russia) to palaeoenvironmental change since ~51.8 ka BP, Quat. Sci. Rev., 247, 106607, https://doi.org/10.1016/j.quascirev.2020.106607, 2020.

1385 Wang, R., Zhang, Y., Wuennemann, B., Biskaborn, B.K., Yin, H., Xia, F., Zhou, L., Diekmann, B.: Linkages between Quaternary climate change and sedimentary processes in Hala Lake, northern Tibetan Plateau, China. J. Asian Earth Sci., 107, 140-150, 2015.

1390 Windirsch, T., Grosse, G., Ulrich, M., Schirrmeister, L., Fedorov, A., Konstantinov, P., Fuchs, M., Jongejans, L., Wolter, J., Opel, T., Strauss, J.: Organic carbon characteristics in ice-rich permafrost in alas and Yedoma deposits, central Yakutia, Siberia, Biogeosciences, 17, 3797–3814 https://doi.org/10.5194/bg-17-3797-2020, 2020.

1395 Woolway, R.I., Merchant, C.J.: Worldwide alteration of lake mixing regimes in response to climate change, Nat. Geosci., 12, 271–276, https://doi.org/10.1038/s41561-019-0322-x, 2019.

Yu, Z., Loisel, J., Brosseau, D. P., Beilman, D. W., and Hunt, S. J.: Global peatland dynamics since the Last Glacial Maximum, Geophys. Res. Lett., 37, L13402, https://doi.org/10.1029/2010GL043584,
1400 2010.

Zhuravlev, G.F., Kazymin, S.S., Pukalo, P.V.: State geological map of the Russian Federation, scale 1:200 000, Anjuyjsker-Chaunsker Series. Moscow (St. Petersburg)., 1999.